Eddy Activity Response to Global Warming–Like Temperature Changes

JANNI YUVAL

Department of Earth, Atmospheric, and Planetary Sciences, Massachusetts Institute of Technology,
Cambridge, Massachusetts

YOHAI KASPI

Department of Earth and Planetary Sciences, Weizmann Institute of Science, Rehovot, Israel

ABSTRACT

Global warming projections show an anomalous temperature increase both at the Arctic surface and at lower latitudes in the upper troposphere. The Arctic amplification decreases the meridional temperature gradient, and simultaneously decreases static stability. These changes in the meridional temperature gradient and in the static stability have opposing effects on baroclinicity. The temperature increase at the upper tropospheric lower latitudes tends to increase the meridional temperature gradient and simultaneously increase static stability, which have opposing effects on baroclinicity as well. In this study, a dry idealized general circulation model with a modified Newtonian cooling scheme, which allows any chosen zonally symmetric temperature distribution to be simulated, is used to study the effect of Arctic amplification and lower-latitude upper-level warming on eddy activity. Due to the interplay between the static stability and meridional temperature gradient on atmospheric baroclinicity changes, and their opposing effect on atmospheric baroclinicity, it is found that both the Arctic amplification and lower-latitude upper-level warming could potentially lead to both decreases and increases in eddy activity, depending on the exact prescribed temperature modifications. Therefore, to understand the effect of global warming–like temperature trends on eddy activity, the zonally symmetric global warming temperature projections from state-of-the-art models are simulated. It is found that the eddy kinetic energy changes are dominated by the lower-latitude upper-level warming, which tends to weaken the eddy kinetic energy due to increased static stability. On the other hand, the eddy heat flux changes are dominated by the Arctic amplification, which tends to weaken the eddy heat flux at the lower levels.

1. Introduction

Due to the increase in greenhouse gas concentration in the atmosphere, atmospheric temperatures are predicted to increase. Climate models project an increase in temperatures that is not spatially uniform, and both meridional and vertical temperature gradients are expected to change in a global warming scenario. Changes in temperatures and especially in temperature gradients lead to changes in atmospheric stability and may lead to large-scale changes in atmospheric circulation. Global warming simulations show anomalous and robust temperature trends in three main regions of the atmosphere (Fig. 1a): 1) an enhanced warming aloft in the tropics, 2) a surface polar amplification in the Northern

Hemisphere (NH), and 3) stratospheric cooling. These temperature trends occur in all climate models used for the Fifth Assessment Report (AR5) of the Intergovernmental Panel on Climate Change (IPCC), though the exact temperature amplitude change varies between models (Vallis et al. 2015). The tropical warming aloft can be attributed to the decrease in the saturated lapse rate with increased water vapor following warming (Manabe and Wetherald 1980), combined with the fact that in the tropics the moist static stability stays close to zero. The large warming in the Arctic has been attributed to different factors such as the ice albedo feedback (Manabe and Stouffer 1980), increased heat transport (Cai 2005, 2006), and changes in longwave radiation (Bintanja et al. 2011). The cooling of the stratosphere is caused by the large increase in emission compared to the small increase in absorption when CO_2 concentration in the stratosphere increases (Ramaswamy et al. 2001; Vallis et al. 2015).

Global warming–like temperature changes might lead to large-scale changes in the atmospheric circulation.

ⓐ Denotes content that is immediately available upon publication as open access.

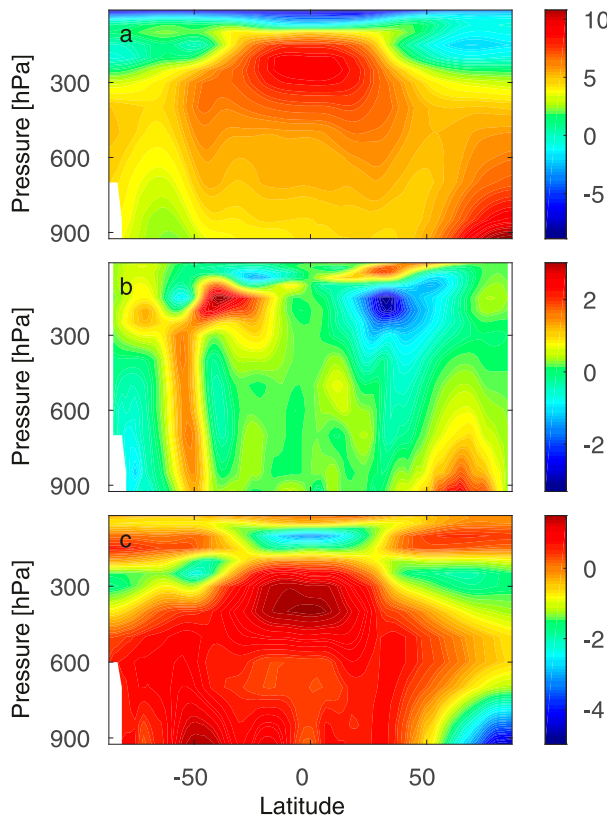*Corresponding author*: Janni Yuval, yaniyuval@gmail.com

FIG. 1. Global warming temperature trends. The mean difference between December–February (DJF) of the last 20 years of the twenty-first century (2081–2100) to the last 20 years of the twentieth century (1981–2000) for the RCP8.5 scenario taken from 10 CMIP5 models (the models that were used for this figure were MRI CGCM3, MPI-ESM-LR, MIROC-ESM, MIROC5, IPSL-CM5A-MR, IPSL-CM5A-LR, HadGEM2-ES, HadGEM2-CC, CSIRO-Mk3.6.0, and CMCC-CM; expansions of acronyms are available online at http://www.ametsoc.org/PubsAcronymList) for (a) temperature (K), (b) the meridional temperature gradient (K m$^{-1} \times 10^{-6}$, $\partial T/a\partial\phi$, where ϕ is the latitude and a is Earth's radius), and (c) the Brunt–Väisälä frequency [s$^{-1} \times 10^{-3}$, $N = (g\partial_z\theta/\theta)^{1/2}$, where g is Earth's gravity, θ is the potential temperature, and ∂_z is the derivative with respect to height].

For example, models show a robust poleward shift in storm tracks and change in their intensity in the Southern Hemisphere (SH; e.g., Held 1993; Stephenson and Held 1993; Hall et al. 1994; Bengtsson and Hodges 2006; Yin 2005; O'Gorman and Schneider 2008; Wu et al. 2010; O'Gorman 2010; Chang et al. 2012; Tamarin-Brodsky and Kaspi 2017). Storm tracks play a fundamental part in the global circulation (e.g., Chang et al. 2002), and therefore it is crucial to understand future changes in their position and intensity.

Several mechanisms were suggested to explain the poleward shift of the storm tracks. Lorenz and DeWeaver (2007) showed in idealized simulations that an increase of the tropopause height, which is a robust result of global warming simulations (Vallis et al. 2015), leads to a poleward shift. Lu et al. (2008) and Lim and Simmonds (2009) suggested that the increase in the subtropical static stability pushes the baroclinic zone poleward, and leads to a poleward shift. Chen et al. (2008) suggested that the shift can be caused by increased phase speed of midlatitude eddies in a climate change scenario (see also Lorenz 2014). Kidston et al. (2011) suggested that increased eddy length scale will lead to a poleward shift. Tamarin-Brodsky and Kaspi (2017) suggested that a more tilted and poleward path of the storms themselves leads to an overall poleward shift of the zonal mean storm track. Voigt and Shaw (2016) and Li et al. (2019) used idealized GCM and showed that changes in cloud radiative effects in global warming simulations contribute to the poleward shift of the extratropical jet. These mechanisms provided the theoretical framework to understand how climate change temperature projections might affect the storm tracks in the SH.

The changes in the position and intensity of the NH storm track are less clear (Chang et al. 2012; Vallis et al. 2015). Besides the more complicated orography in the NH, which leads to large zonal asymmetries, the projected temperature trends in the NH are more complex. For example, the meridional temperature gradients at the lower and upper troposphere have opposite trends. At the lower troposphere, the temperature gradient reduces due to polar amplification, but in the upper troposphere the gradient increases due to the upper tropical heating (Fig. 1b). Motivated by the projected trends, Held and O'Brien (1992), Pavan (1996), Lunkeit et al. (1998), Wu et al. (2012), and Yuval and Kaspi (2016) have studied whether the upper or lower temperature gradient plays a more important role in affecting eddy activity in various complexity of models. These studies have mainly focused on the changes in meridional gradient at different levels.

In this study we emphasize that it is not possible to modify the meridional temperature gradient at specific vertical levels (nonuniformly with height) without affecting the lapse rate.[1] The baroclinicity is affected by both the static stability (which is proportional to the lapse rate) and the meridional temperature gradient. For example, the Eady growth rate (Eady 1949), which is commonly used as a measure of baroclinicity, is proportional to $\partial_y T/N$, where N is the Brunt–Väisälä frequency and $\partial_y T$ is the meridional temperature gradient. Therefore, changes in both the meridional temperature

---

[1] If $\partial_y T = f(z)$, where $f(z)$ is explicitly dependent on z, it necessarily implies that $\partial_z T \neq 0$.

gradient and the Brunt–Väisälä frequency (which is proportional to the square root of the static stability) should be taken into account when studying the response of eddy activity to temperature changes. For example, when the meridional temperature gradient decreases at the lower levels due to the Arctic amplification (Fig. 1b), the Brunt–Väisälä frequency decreases at the same time (Fig. 1c). Therefore, the decreased temperature gradient and decreased Brunt–Väisälä frequency have an opposite effect on the baroclinicity. Since both the meridional temperature gradient and the static stability affect baroclinicity, it is not straightforward to determine whether the Arctic amplification leads to increase or decrease in baroclinicity. As we show in this study, decreasing the lower-level temperature gradient via an increase in lower-level Arctic temperatures could lead to an increase or decrease in eddy activity, depending on the exact temperature modifications.[2] In the case of upper tropospheric tropical heating, the meridional temperature gradient changes and the (dry) static stability changes have an opposite effect on the baroclinicity in the subtropics. While the meridional temperature gradient increases and tends to enhance baroclinicity, the Brunt–Väisälä frequency (and static stability) increases and tends to decrease baroclinicity (Fig. 1).

In this study we use an idealized general circulation model (GCM) with a modified Newtonian relaxation scheme to study the effect of zonally symmetric increased lower-level Arctic temperatures, and zonally symmetric increased upper tropical tropospheric temperatures on eddy activity. Many previous studies used idealized GCMs to investigate the effects of global warming–like temperature changes on the atmospheric circulation. These studies focused on inducing diabatic heating changes that resemble the change in the temperature trends predicted by the IPCC report (e.g., Polvani and Kushner 2002; Kushner and Polvani 2004; Lorenz and DeWeaver 2007; Lim and Simmonds 2009; Butler et al. 2010; Lu et al. 2014). These studies have contributed to our understanding of how global warming–like temperature trends could affect the circulation. For example, Butler et al. (2010) used an idealized GCM with a Newtonian cooling scheme, and modified the relaxation temperature such that it will represent upper tropospheric tropical warming and low-level polar heating. They found that upper tropospheric tropical warming tends to shift storm track poleward

while low-level polar heating leads to an opposite tendency (and hence there is a competition between the two effects).

One limitation of these studies is that instead of reproducing the projected global warming–like temperature changes, these studies prescribe an increased (or decreased) diabatic heating in regions that are projected to have anomalous temperature changes. However, inducing diabatic warming at a certain region may lead to temperature changes also in other regions due to temperature advection [e.g., see Fig. 2 in Butler et al. (2010), where the polar lower stratosphere is cooled when the upper tropics are warmed]. Therefore, it is not straightforward to obtain temperature changes that resemble a global warming–like temperature changes by adding diabatic heating terms, and to systematically investigate the effect of different temperature changes on atmospheric circulation. Nevertheless, controlling changes in diabatic heating or controlling temperature changes (by simulating a specified temperature field) could be both useful methods to study the circulation response to global warming–like changes. Since most of the theoretical explanations to the response of eddy fields in a climate change scenario rely on the projected temperature field changes, and not on the diabatic heating changes, and since most idealized studies focus on controlling the diabatic heating, we find it important to study the response of eddy activity to global warming–like changes in idealized framework where the mean temperature can be prescribed in simulations.

It is found in this study that the details of the exact temperature changes could lead to very different responses of eddy activity. Therefore, it is important to understand the eddy sensitivity to the shape of temperature changes, and be able to represent accurately the projected temperatures from a global warming scenario. We note that the response of dynamic variables is very sensitive to the specific details of warming even in comprehensive GCMs, and not unique to idealized GCMs. For example, Liu et al. (2012) and Screen et al. (2014) used two identical models and almost identical forcings and yet the response of sea level pressure due to Arctic amplification in their models was different.

The paper is organized as follows. The idealized GCM and the modified Newtonian relaxation scheme are presented in section 2a. The modified temperature profiles used to simulate global warming–like temperature trends in the idealized GCM are discussed in sections 2b and 2c. The simulations results using a hemispherically symmetric reference state with enhanced upper tropospheric temperature gradient and reduced lower-level temperature gradient are discussed in sections 3a and 3b. In these sections, the competing effects of static stability

---

[2] Also Lunkeit et al. (1998) and Yuval and Kaspi (2016) showed an increase in EKE due to decreased temperature gradient due to polar warming. We discuss and explain these results in section 5.

changes and meridional temperature gradient are investigated. In section 3c idealized simulations with simultaneous temperature changes in the upper tropical troposphere and the polar surface are discussed. Next, using a more ''realistic'' zonally symmetric reference state with temperature modifications taken directly from the representative concentration pathway 8.5 (RCP8.5) simulations, the circulation response to Arctic amplification and tropical upper tropospheric temperature increase are studied (section 4). The results are discussed and summarized in section 5.

2. Methods

A dry version of an idealized GCM based on the spectral dynamical core of the GFDL Flexible Modeling System (FMS) is used. The model is driven by a Newtonian cooling scheme that is described in section 2a. The simulations do not include orography or ocean, and dissipation in the boundary layer is represented by linear damping of near-surface winds (below $\sigma = 0.7$) with a relaxation time of 1 day at the surface [see Held and Suarez (1994) for details]. All simulations have 60 vertical sigma levels with a T42 ($2.8° \times 2.8°$) horizontal resolution. What distinguishes our simulations from Held and Suarez (1994) is the relaxation temperature distribution and the different relaxation time used for the zonal mean and the eddies in the temperature equation (see section 2a). Throughout this study, unless stated explicitly otherwise, eddy fields are defined as a deviation from the zonal and time mean.

All simulations except the reference simulations are integrated over 3000 days, where the first 500 days of each simulation are treated as spinup, and the results are averaged over the last 2500 days. The reference simulations were integrated over 9000 days and results are averaged over the last 8500. In section 3 all the simulations are hemispherically symmetric and results are presented after averaging over both hemispheres. In section 4 the simulations are not hemispherically symmetric and we present results from both hemispheres or only for the NH, depending on the context.

a. Forcing the mean state

To modify the temperature field such that it resembles a climate change–like temperature changes, a Newtonian cooling scheme suggested by Zurita-Gotor and Lindzen (2006) and Zurita-Gotor (2007) is used. The main difference between this method and other heating formulations used in idealized models is the usage of different relaxation time scales for the eddies and the zonal mean. The temperature equation in this formulation can be written as

$$\partial_t T = \cdots - \alpha_T^{-1}(T - \overline{T}) - \alpha_T^{-1}\gamma(\overline{T} - T_R), \quad (1)$$

where $\overline{A}$ is the zonal mean of field A, α_T is the relaxation time of eddies, chosen to be as in Held and Suarez (1994), and $\alpha_T\gamma$ is the relaxation time for the mean state, where we take $\gamma = 100$; also, T_R is the relaxation temperature and described in section 2b. The fast relaxation time of the zonal mean state is chosen to allow reproduction of any chosen target temperature profile with a good accuracy (choosing a significantly smaller value for γ results in large differences between the relaxation temperature and the simulation temperature). Using Eq. (1) in simulations leads to a close similarity between the zonal and time mean temperature and the relaxation temperature (for a comparison between a relaxation temperature and a simulation temperature, see Fig. A1a in appendix A). This allows us to study how eddy activity responds to global warming–like temperature changes (e.g., Arctic amplification and upper tropospheric tropical warming) and to test the sensitivity of eddy activity changes when different temperature profiles are simulated. A discussion regarding the possible drawbacks of strong zonal temperature relaxation can be found in appendix D herein, and in Yuval and Kaspi (2017, 2018), where it is shown that using another method that allows controlling the mean temperature distribution, and does not use different relaxation time scales for the eddies and zonal mean, yields similar eddy fields differences as the method used here. We stress that the aim of this study is to understand what part of the circulation response could be explained by the zonally symmetric temperature changes, and to deepen the understanding of the competing roles of changes in the static stability and the meridional temperature gradient. Therefore, we choose to focus on zonally symmetric simulations, rather than on a more realistic setting that includes moisture or orography, although these components play an important role in Earth's atmospheric circulation (Pithan et al. 2016; Wills and Schneider 2016, 2018; Wu and Reichler 2018).

b. Relaxation temperature profiles—Hemispherically symmetric simulations

In this study we focus on the effect of the anomalous temperature increase at the tropical upper troposphere and at the polar surface. To consider a global warming–like temperature changes in the upper troposphere, the reference temperature was modified as follows:

$$\delta T_{\text{tropical}} = -A^{\text{upper}} \times e^{[-(\sigma-\sigma_c^{\text{upper}})^2/(2\sigma_w^{\text{upper}})^2]}$$
$$\times \left[\tanh\left(\frac{|\phi| - \phi_c^{\text{upper}}}{\phi_w^{\text{upper}}}\right) - 1\right], \quad (2)$$

where $2 \times A^{\text{upper}}$ is the amplitude of the temperature change, ϕ is the latitudinal coordinate, ϕ_c^{upper} determines the latitude where the temperature gradient is centered, ϕ_w^{upper} determines the temperature gradient width, σ is the vertical coordinate, σ_c^{upper} is the vertical level with maximal temperature changes, and σ_w^{upper} determines the vertical width of the temperature changes. The relaxation temperature in simulations with tropical upper tropospheric temperature changes is $T_R = T_{\text{ref}}^{\text{HS}} + \delta T_{\text{tropical}}$, where $T_{\text{ref}}^{\text{HS}}$ is the reference temperature. The reference temperature was chosen to be the mean temperature of a simulation with the Held and Suarez (1994) forcing. The Newtonian cooling scheme presented in Eq. (1) was used with this reference temperature ($T_{\text{ref}}^{\text{HS}}$) as its relaxation temperature to determine the reference simulation for all the simulations presented in section 3. The tanh function, which parameterizes the latitudinal shape of the heating, is preferred over an exponential dependence because it produces a sharper meridional gradient, which is similar to the projected gradient changes in global warming simulations (where the gradient change is concentrated in subtropics/midlatitudes and not inside the tropics; Fig. 1a).

The temperature differences between the reference simulation and simulations with increased tropical upper tropospheric temperature field with the parameters $A = 2\,\text{K}$, $\sigma_w^{\text{upper}} = 0.11$, $\phi_c^{\text{upper}} = 35°, 40°, 45°, 50°$, $\sigma_c^{\text{upper}} = 0.3$, and $\phi_w^{\text{upper}} = 10°$ are shown in Figs. 2a–d. The modifications of ϕ_c^{upper} allows us to investigate the interplay between the effect of the static stability and the meridional temperature gradient on the eddy fields. Larger ϕ_c^{upper} values tend to modify the static stability in a broader region, while shifting the latitudinal location of the meridional temperature gradient but keeping its magnitude unaffected (appendix A). To investigate the sensitivity of eddy activity to changes in the center level of warming (σ_c) simulations with all the combinations of $A^{\text{upper}} = 2\,\text{K}$, $\sigma_w^{\text{upper}} = 0.11$, $\phi_c^{\text{upper}} = 30°$, $35°, 40°, 45°, 50°, 55°$, $\sigma_c^{\text{upper}} = 0.2, 0.3, 0.4$, and $\phi_w = 10°$ were conducted (18 simulations). Since the results presented in section 3a are qualitatively robust to these changes, these simulations are not shown.

To consider Arctic amplification–like temperature changes, the target temperature was modified as follows:

$$T_{\text{arctic}} = A^{\text{lower}} \left\{ 1 + \tanh\left[2\frac{\text{abs}(\phi) - \phi_c^{\text{lower}}}{\phi_w^{\text{lower}}} \right] \right\} e^{-(\sigma-1)^2/(2\sigma_w^{\text{lower}})^2},$$

(3)

where the parameters have similar meaning as in Eq. (2) (superscripts changed from upper to lower), but the temperature modification is concentrated at the polar surface. The temperature differences between the reference simulation and simulations with Arctic amplification–like

temperature changes [using Eq. (3)] with the parameters $A^{\text{lower}} = 2\,\text{K}$, $\sigma_w^{\text{lower}} = 0.2$, $\phi_w^{\text{lower}} = 30°$, and $\phi_c^{\text{lower}} = 40°, 50°, 70°, 80°$ are shown in Figs. 3a–d. Similarly to the case of upper tropospheric temperature gradient modifications, changes in ϕ_c^{lower} allow the investigation of the interplay between the effect of the static stability and of the meridional temperature gradient on eddy fields.

To verify the robustness of the results presented in section 3b, we conducted simulations with the parameters $A^{\text{lower}} = 2\,\text{K}$, $\sigma_w^{\text{lower}} = 0.1, 0.2$, and $\phi_w^{\text{lower}} = 10°, 20°, 30°$ and all the combinations with $\phi_c^{\text{lower}} = 10°, 20°, 30°, 40°, 50°, 60°, 70°, 80°$ (48 simulations). The modifications in ϕ_w^{lower} and σ_w^{lower} are used to test the robustness of the qualitative conclusions when ϕ_c^{lower} is modified. Since the qualitative results of the additional simulations are similar to the results presented in section 3b, these simulations are not shown.

c. Relaxation temperature profiles—ECMWF reference

To simulate more realistic global warming temperature changes, temperature modifications that are quantitatively similar to the projections obtained from phase 5 of the Coupled Model Intercomparison Project (CMIP5) are used to modify a chosen reference state. To consider a realistic reference temperature, the reference relaxation temperature is chosen to be the zonal and wintertime (DJF) mean temperature obtained from the European Centre for Medium-Range Weather Forecasts (ECMWF) interim reanalysis (ERA-Interim) dataset between the years 1979 and 2014 ($T_{\text{ref}}^{\text{ECMWF}}$). We find it important to use a reference state that resembles Earth's circulation since different reference states might respond differently to the same temperature changes (section 4 and section a of appendix C). Therefore, a reference state that resembles an Earth-like circulation more than the Held and Suarez (1994) reference is chosen. The relaxation temperature was modified as follows:

$$T_{\text{RCP85}}^{\text{ECMWF}} = T_{\text{ref}}^{\text{ECMWF}} + T_{\text{RCP85}}^{\text{mod}},$$

(4)

where $T_{\text{RCP85}}^{\text{mod}}$ is the difference between the RCP8.5 temperature projections to the historical temperatures (shown in Fig. 5a).

To better understand the effect of "realistic" upper tropospheric tropical heating on the eddy fields in the NH, the ECMWF reference temperature was modified such that it will approximately reproduce the meridional temperature gradients that are projected to occur in an RCP8.5 scenario at the upper troposphere. The focus mainly on the NH is because the effect of global warming temperature trends on the large-scale circulation is less
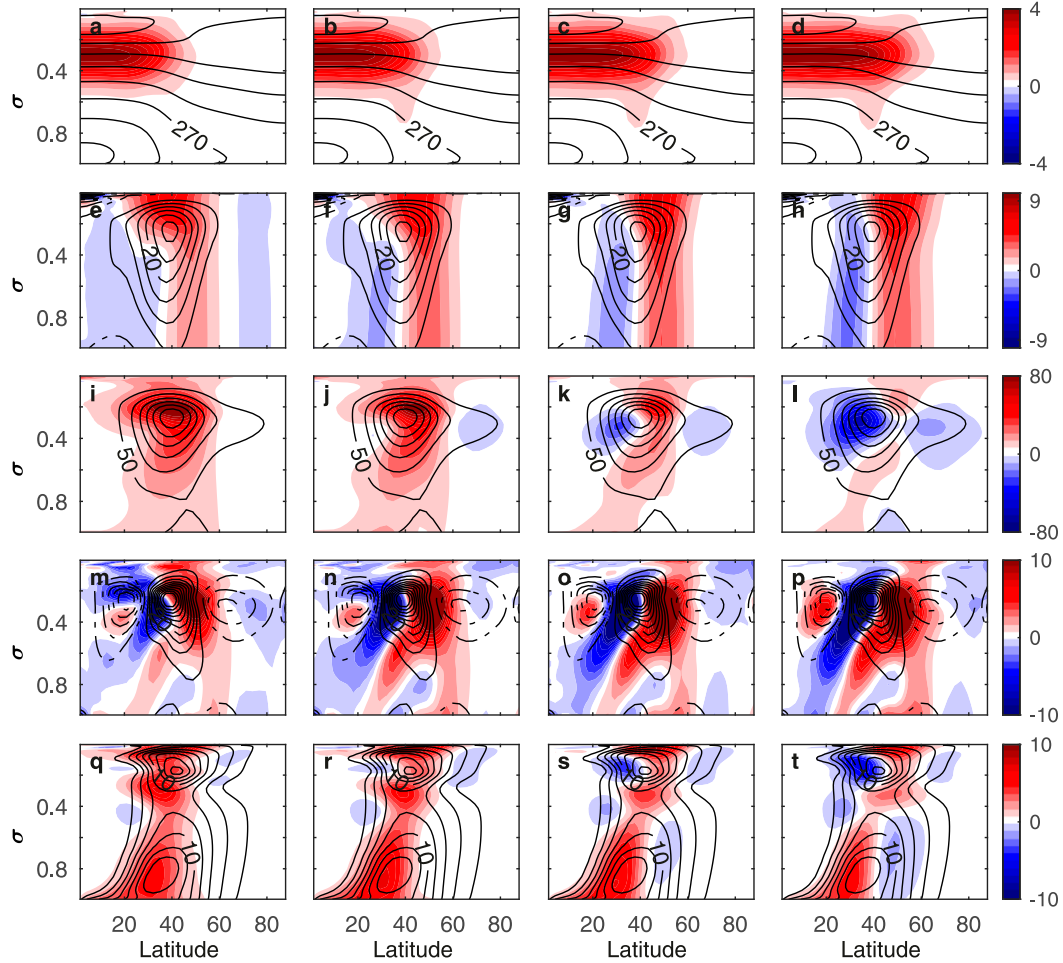
FIG. 2. The zonal wind and eddy fields response to temperature increase at low latitudes of the upper troposphere in an idealized GCM: (a)–(d) temperature, (e)–(h) zonal wind, (i)–(l) EKE, (m)–(p) EMFC $\times 10^6$, and (q)–(t) EHF for simulations that the upper troposphere was modified with tropical upper tropospheric temperature increase as in Eq. (2) using the parameters $A^{\text{upper}} = 2\,\text{K}$, $\phi_c^{\text{upper}} = 35°$, $40°$, $45°$, $50°$, $\phi_w^{\text{upper}} = 10°$, $\sigma_c^{\text{upper}} = 0.3$, and $\sigma_w^{\text{upper}} = 0.11$. Colors indicate the deviation from the reference simulation and contours show the reference simulation fields. The contour intervals are 15 K (temperature), 5 m s^{-1} (zonal wind), 50 m^2 s^{-2} (EKE), 5 m s^{-2} (EMFC), and 2 K m s^{-2} (EHF). Colors have the same units as contours.

clear in the NH compared to the SH. The temperature was modified in the following manner:

$$\delta T_{\text{tropical}}^{\text{ECMWF}}(0° \le \phi \le \phi_c^{\text{tropical}})$$
$$= e^{-(\sigma - \sigma_c)^2/2\sigma_w^2} \int_\phi^{0°} \partial_{\phi_0}(T_{\text{RCP85}}^{\text{mod}})\, d\phi_0, \qquad (5)$$

where $\delta T_{\text{tropical}}^{\text{ECMWF}}(\phi > \phi_c^{\text{tropical}}) = 0°$ and $\delta T_{\text{tropical}}^{\text{ECMWF}}(\phi < 0°) = \delta T_{\text{tropical}}^{\text{ECMWF}}(\phi > 0°)$, and ∂_{ϕ_0} is the derivative with respect to the latitudinal coordinate. The exponential decay of the temperature changes with the vertical coordinate is chosen in order to limit the temperature changes to the upper troposphere. We take $\sigma_c = 0.25$ since it is the vertical level that the temperature modification is largest, and $\sigma_w = 0.4$ (smaller values of σ_w

limit the temperature changes to fewer levels, while larger values lead to temperature cooling in the lower levels) The parameter ϕ_c^{tropical} determines the largest latitude where the temperature modifications occur, and is qualitatively similar to the parameter ϕ_c^{upper} in Eq. (2). The latitudinal width of the temperature extent is modified ($\phi_c^{\text{tropical}} = 25°$, $30°$, $35°$, $40°$, $45°$, $50°$, $55°$, $60°$, $65°$) to investigate the effect of the meridional temperature gradient width on the circulation (section 4a).

To study the effect of the Arctic amplification in the NH on eddy fields, the ECMWF reference state was modified such that

$$\delta T_{\text{Arctic}}^{\text{ECMWF}}(\phi \ge \phi_c^{\text{Arctic}}) = e^{-(\sigma-1)^2/2\sigma_w^2} \int_\phi^{90°} \partial_{\phi_0}(T_{\text{RCP85}}^{\text{mod}})\, d\phi_0,$$
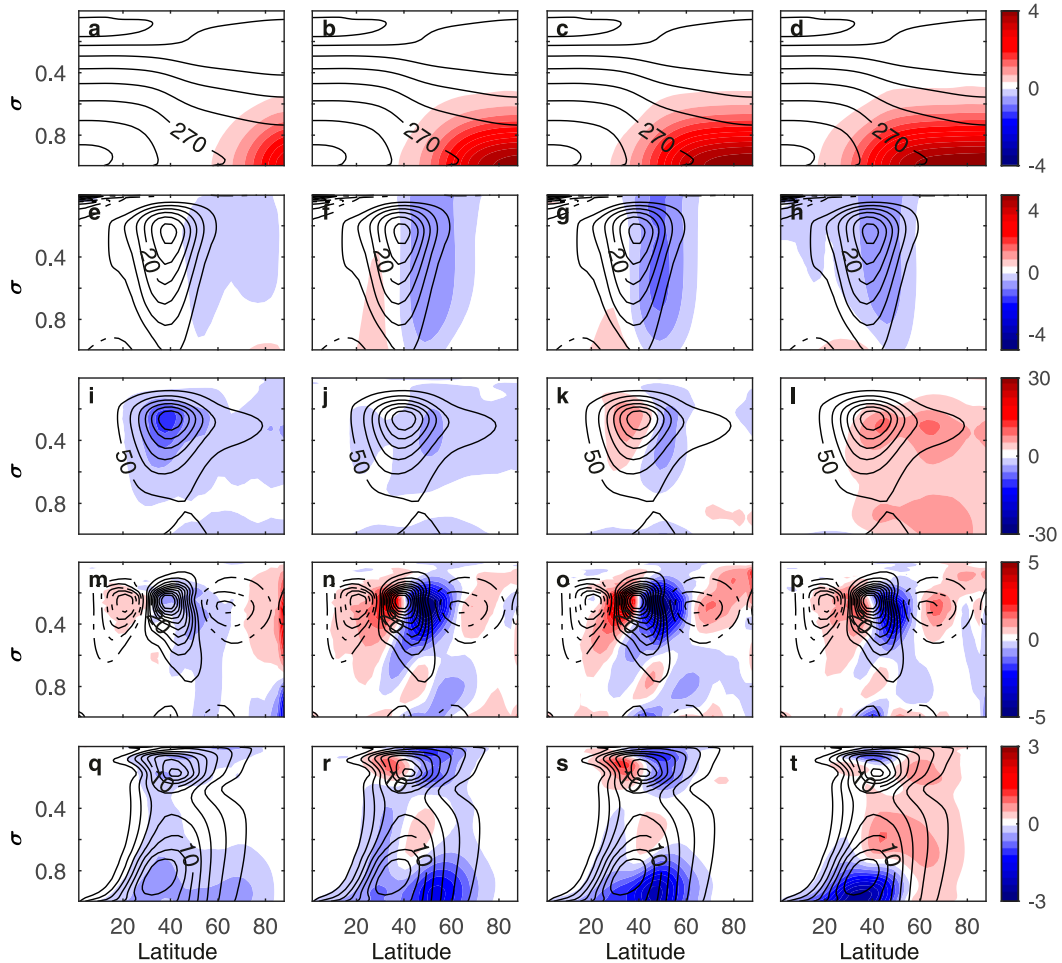$$(6)$$

FIG. 3. The zonal wind and eddy fields response to polar surface temperature increase in an idealized GCM: (a)–(d) temperature, (e)–(h) zonal wind, (i)–(l) EKE, (m)–(p) EMFC × 10⁶, and (q)–(t) EHF for Arctic amplification–like simulations. The temperature modifications are calculated from Eq. (3), using the parameters $A^{\text{lower}} = 2K$, $\phi_c^{\text{lower}} = 40°, 50°, 60°, 80°$, $\phi_w^{\text{lower}} = 30°$, and $\sigma_w^{\text{lower}} = 0.2$. Colors indicate the deviation from the reference simulation and contours show the reference simulation fields. The contour intervals are 15 K (temperature), 5 m s⁻¹ (zonal wind), 50 m² s⁻² (EKE), 5 m s⁻² (EMFC), and 2 K m s⁻² (EHF). Colors have same units as contours.

and $\delta T_{\text{Arctic}}^{\text{ECMWF}} = 0$ elsewhere. We take $\sigma_w = 0.4$, such that the gradient changes are limited mostly to the lower levels. The parameter ϕ_c^{Arctic} determines the lowest latitude that the temperature modifications occur, and plays a similar role as the parameter ϕ_c^{lower} in Eq. (3). The parameter ϕ_c^{Arctic} was varied in order to investigate its effect on the eddy fields ($\phi_c^{\text{Arctic}} = 30°, 35°, 40°, 45°, 50°, 55°, 60°, 65°, 70°$). We note that the qualitative results presented in this study are reproduced also when using a reference simulation with the historical CMIP5 DJF temperature distribution (from the models averaged in Fig. 1) instead of the ECMWF reference.

3. Results with hemispherically symmetric simulations

In this section, the results of idealized hemispherically and zonally symmetric simulations with global

warming–like temperature modifications are presented. We focus on the response of eddy fields to two robust anomalous temperature changes occurring in global warming simulations: low-latitude upper tropospheric temperature increase (section 3a) and Arctic amplification (section 3b).

a. Upper tropospheric low-latitude temperature increase

When the low-latitude upper tropospheric temperature increases, there are changes in baroclinicity due to the increased meridional temperature gradient and the increased static stability. To focus on the interplay between the changes in the meridional temperature gradient and the static stability, the latitudinal extent of the simulated temperature changes has been modified

[the parameter ϕ_c^{upper} in Eq. (2)]. The changes in the latitudinal extent of the temperature field are used in order to investigate the sensitivity of eddy activity response to the shape of the temperature modifications. As the width of the temperature modification increases (ϕ_c^{upper} increases from left to right in Fig. 2), the Brunt–Väisälä frequency increases at the upper troposphere in a broader region (see also Figs. A1i–l, appendix A) and decreases in the lower stratosphere.[3] Simultaneously, the meridional temperature gradient changes are pushed more poleward (Figs. A1e–h), but its overall mean magnitude is approximately unchanged.

All simulations in Fig. 2 show a poleward shift of the jet, which is a robust result of global warming simulations in the SH, and is obtained in most CMIP5 models also in the NH (Vallis et al. 2015). Furthermore, the eddy momentum flux convergence (EMFC) has a similar qualitative response in all simulations: larger convergence at the poleward flank of the jet and decreased convergence at the equatorward flank of the jet (Figs. 2m–p), leading to a poleward shift of the surface westerlies in all simulations (Figs. 2e–h). The eddy kinetic energy (EKE; Figs. 2i–l) and eddy heat flux (EHF; Figs. 2q–t) response to low-latitude upper tropospheric temperature increase varies significantly as the temperature gradient is modified at different latitudes. As the latitudinal extent of the temperature increases, the warming is not limited to the tropics, and penetrates deep into the extratropics. When the temperature increase is limited to lower latitudes, the response of the EKE and EHF is positive (Figs. 2i,j), but when the temperature increase penetrates deep into the extratropics, the response changes sign in some regions (Figs. 2k,l).

The EKE and EHF response when the latitudinal extent of the temperature modification is broadened can be explained by the interplay between the static stability and meridional temperature gradient changes. As the latitudinal extent of the temperature gradient is broadened, the static stability increase spans over a larger region (Fig. B1) and tends to decrease eddy activity more effectively, while the meridional temperature gradient magnitude remains approximately constant. Furthermore, the latitudinal location of the gradient changes can play an important role in the eddy activity response (Yuval and Kaspi 2018). When the extent of the warming is pushed significantly poleward (Fig. 2d),

the gradient is modified at the outskirts of the baroclinic region, and probably has less an effect on eddy activity. Simultaneously, the static stability increase inside the baroclinic region tends to weaken eddy activity. The same qualitative results are reproduced when the vertical location of the warming is modified ($\sigma_c^{\text{upper}} = 0.2, 0.3, 0.4$; not shown).

In appendix B it is demonstrated that when the meridional temperature gradient is modified with identical changes as in Fig. 2, but it is done by high-latitude cooling, the response of the eddy fields is always strengthening, and with much larger amplitude than in Fig. 2. Since the meridional temperature gradient is identical in Fig. 2 (and in Fig. B1 in appendix B) but the static stability changes are different, we conclude that these large differences in the response are due to the different changes in static stability.

b. Arctic amplification temperature changes

An increase in the surface temperature at higher latitudes leads to a decrease in the meridional temperature gradient which acts to decrease baroclinicity. Simultaneously it leads to a decreased static stability which acts to increase baroclinicity. As in section 3a, we focus on the interplay between the changes in the meridional temperature gradient and the static stability. Therefore, the latitudinal extent of the simulated temperature changes is modified [the parameter ϕ_c^{lower} in Eq. (3)]. As the width of the temperature modification increases (ϕ_c^{lower} decreases from left to right in Fig. 3), static stability decreases close to the surface in a larger region, and the meridional temperature gradient decrease is pushed toward lower latitudes, but its overall mean magnitude is approximately unchanged.

The EKE (Figs. 3i–l) and EHF (Figs. 3q–t) responses to high-latitude surface temperature increase vary significantly as the temperature gradient is modified at different latitudes. As the latitudinal extent of the temperature change increases toward lower latitudes, the warming is not limited to the polar regions and it penetrates deeply into the extratropics. When the temperature changes are constrained to higher latitudes, the EKE and EHF response is negative (Figs. 3i,j). Differently, when the temperature changes occur also at lower latitudes, the responses of the EKE and EHF become partly positive (Figs. 3k,l).

As discussed in section 3a, these trends can be explained by the interplay between the static stability and meridional temperature gradient changes. The results obtained in this section imply that the effect of a reduction in the meridional temperature gradient on eddy activity can be weaker than the effect of the static stability decrease when the static stability is modified in a

---

[3] The decrease in static stability occurs at high altitudes that are within the stratosphere, and it therefore plays relatively a minor role in changing the tropospheric eddy activity in the idealized model used in this study (which does not have a realistic stratospheric circulation). Therefore, these changes are not highlighted in the manuscript.

sufficiently large region (e.g., Fig. 3l). Furthermore, in section 5 it is discussed how these results could potentially explain a previous result obtained by Lunkeit et al. (1998).

In appendix B2 it is demonstrated that when the meridional temperature gradient is modified with identical changes as in Fig. 3, but it is done by low-latitude warming, the response of the eddy fields is always weakening, and with much larger amplitude than in Fig. 3. Since the meridional temperature gradient is identical in Fig. 3 (and in Fig. B2 in appendix B) but the static stability changes are different, we conclude that these large differences in the response are due to the different changes in static stability. We note that the qualitative results described in this section are also obtained for other parameter choices (all the combinations of $\phi_w^{\text{lower}} = 10°$, $20°$, $30°$ and $\sigma_w^{\text{lower}} = 0.1$, 0.2 were simulated with a gradual change in ϕ_c^{lower}).

c. Combined experiments

In this section, the eddy fields' response to a simultaneous lower-latitude upper troposphere and surface polar region temperature increase ($T_{\text{combined}} = T_{\text{ref}}^{\text{HS}} + \delta T_{\text{tropical}} + \delta T_{\text{arctic}}$) is investigated. There are many different parameter combinations that could be chosen to simulate a simultaneous changes at the polar surface region and at the upper troposphere. In Fig. 4 only two such choices are shown. The parameter combinations that are used lead to temperature changes that have some resemblance to global warming–like temperature gradients obtained in projections. Namely, the positions of the meridional temperature gradients, both in the upper troposphere and in the lower troposphere, are located at the same regions as in the projections, and their relative positions are similar to the projections (Fig. 1b). The simulations shown in Fig. 4 have a relatively similar temperature changes but nevertheless show a qualitatively different EKE response (Figs. 4i,j), indicating that the EKE response is sensitive to the exact details of the temperature modifications (seen also in Fig. 2).

The eddy activity and zonal wind response in the combined simulations is almost identical to the linear sum responses of simulations where the lower-latitude upper troposphere and the polar surface are warmed separately (Fig. 4).[4] This implies that the simulated temperature modifications affect the circulation such

that it is in the linear response regime, and the changes in the circulation due to the different temperature changes interact very weakly. Since the response of eddy activity to upper tropospheric changes is larger (cf. Figs. 2 and 3), eddy activity changes are dominated by the upper tropospheric temperature changes in the combined simulations. For example, the response in the first (second) column of Fig. 4 is similar to the response shown in the second (fourth) column of Fig. 2 (where the two simulations have the same upper tropospheric temperature change).

We note that there are many parameters other than the latitudinal extent of the temperature modification, such as the vertical width, the latitudinal width, amplitude, and so on that should be taken into account when considering the similarity of the temperature modifications in the idealized simulation and projections. Therefore, more realistic temperature modifications are considered in section 4, and we do not extend the discussion of whether the results presented in this section necessarily indicates that the upper tropospheric tropical warming modification will affect eddy fields more than the Arctic warming, and discuss this question in more detail in section 4.

4. Results with an ECMWF-like reference state

The results of section 3 highlighted the interplay between changes in the static stability and meridional temperature gradient. Building on the results of section 3, in this section, the eddy fields and zonal wind response to global warming–like temperature changes are studied using a more "realistic" zonally symmetric reference temperature taken from the ECMWF (section 2c). Since the eddy response to a specific temperature modification might be affected from the reference state, it is important to study the response using a reference state that is similar to Earth. This point is demonstrated in appendix C1, where it is shown that when the Held and Suarez (1994) reference ($T_{\text{ref}}^{\text{HS}}$) is modified using the temperature trends from the RCP8.5 scenario ($T_{\text{RCP85}}^{\text{mod}}$), the eddy response is qualitatively different compared to similar changes applied to the ECMWF zonally symmetric reference ($T_{\text{ref}}^{\text{ECMWF}}$, Fig. 5).[5]

The temperature, zonal wind, EKE, EMFC, and EHF of the ECMWF zonally symmetric reference simulation are plotted in Fig. 5 (contours). This simulation is hemispherically asymmetric, and since the reference

---

[4] Butler et al. (2010) compared the dynamic response in simulations where they had a simultaneous global warming–like idealized forcing and the sum of responses from separate simulations (each forced at different regions) and had a similar qualitative result.

[5] For a direct comparison between the Held and Suarez (1994) reference and the ECMWF reference used in this study see Fig. C4.
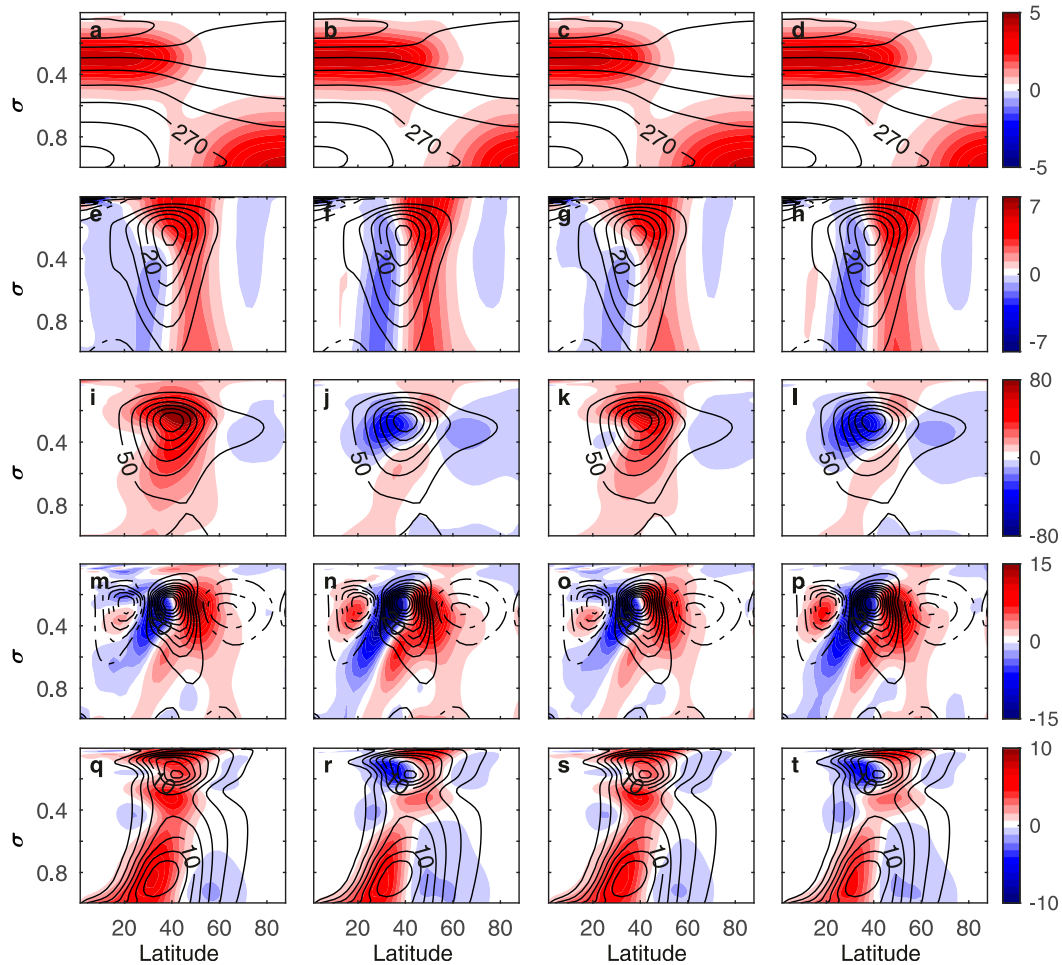
FIG. 4. Comparison between the zonal wind and eddy fields response to simultaneous temperature increase at the low latitudes of the upper troposphere and polar surface to the response from a linear sum of similar temperature changes done in separate simulations: (a)–(d) temperature, (e)–(h) zonal wind, (i)–(l) EKE, (m)–(p) EMFC $\times 10^6$, and (q)–(t) EHF for (two left columns) combined simulations of upper tropospheric tropical warming and Arctic amplification–like simulations and (two right panels) the linear sum of simulations that the tropical upper tropospheric and polar surface are modified separately. The parameter combinations that are chosen for the first and third columns are $A^{lower} = 2$ K, $\phi_c^{lower} = 60°$, $\phi_w^{lower} = 30°$, and $\sigma_w^{lower} = 0.2$ and $A^{upper} = 2$ K, $\phi_c^{upper} = 40°$, $\phi_w^{upper} = 10°$, $\sigma_w^{upper} = 0.11$, and $\sigma_c^{upper} = 0.3$ (for the upper tropical warming). For the second and fourth rows the parameters the parameters are similar except that $\phi_c^{lower} = 70°$ and $\phi_c^{upper} = 50°$ (tropical warming). Colors indicate the deviation from the reference simulation and contours show the reference simulation fields. The contour intervals are 15 K (temperature), 5 m s^{-1} (zonal wind), 50 m^2 s^{-2} (EKE), 5 m s^{-2} (EMFC), and 2 K m s^{-2} (EHF). Colors have same units as contours.

temperature is taken from the NH winter, the temperature gradients as well as the EHF are larger in the NH (Figs. 5a,e). The differences between the ECMWF reanalysis data and the zonally symmetric reference simulation used in this section are discussed in section b of appendix C. In the NH, the simulation has some resemblance to the zonally average reanalysis data, while in the SH there are large differences in EKE and in surface winds (section b of appendix C). Despite the differences between the ECMWF reference and the reanalysis data in the NH, we find it

important to study the response of global warming–like temperature changes in the ECMWF reference, as it still represents an Earth-like circulation better than the Held and Suarez (1994) reference (see section b of appendix C) in the NH.

When the RCP8.5 temperature changes are simulated with the idealized model, the zonal wind in the SH tends to intensify at the poleward flank of the jet, both at the surface and in the upper troposphere (Fig. 5b, colors). A similar poleward jet shift in the SH during DJF is a robust trend in a global warming scenario (e.g., Wu et al.
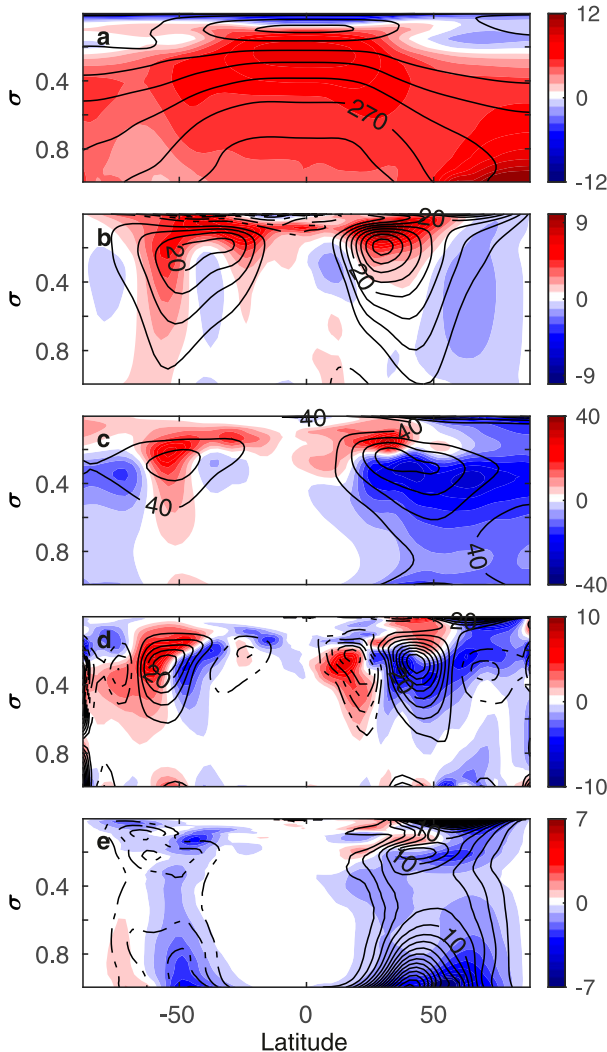
FIG. 5. The zonal wind and eddy fields response in the ECMWF reference simulation to temperature changes taken from projections of the RCP8.5 scenario. Contours show the (a) temperature, (b) zonal wind, (c) EKE, (d) EMFC $\times 10^6$, and (e) EHF for the ECMWF reference temperature ($T_{\text{ref}}^{\text{ECMWF}}$, details in section 2). Colors show the difference between a simulation with the simulated RCP8.5 trends ($T_{\text{RCP85}}^{\text{mod}}$) and the ECMWF reference. The contour intervals are 15 K (temperature), 5 m s^{-1} (zonal wind), 40 m^2 s^{-2} (EKE), 5 m s^{-2} (EMFC), and 2 K m s^{-2} (EHF). Colors have same units as contours.

2010; Vallis et al. 2015). Furthermore, the EKE in the SH is enhanced at the EKE maximal region and slightly poleward to this region, and reduced at the equatorward flank of the jet (Fig. 5c), which is qualitatively similar to projections from CMIP5 simulations (Chang et al. 2012). The reduction of EKE at high latitudes in the SH (Fig. 5c) is not projected in global simulations and could be a result of the lack of orography (i.e., Antarctica) in the idealized model. In the NH the jet tends to

intensify in the upper troposphere at midlatitudes, which is projected in some comprehensive models (Lorenz and DeWeaver 2007), and tends to weaken at higher latitudes (Fig. 5b), which is not projected in models. The weakening of the zonal winds at high latitude is related to the increased eddy momentum flux divergence at high latitudes in the simulation (Fig. 5d). The EKE response in the RCP8.5 idealized simulation in the NH is a general weakening at the mid- to lower troposphere, and an increase in the upper troposphere at lower latitudes. This result is with reasonable qualitative agreement with the CMIP5 ensemble mean modifications, which shows an overall decrease (with low certainty) in the lower troposphere, and an increase in the upper troposphere/ lower stratosphere (Chang et al. 2012). Furthermore, the idealized model is missing a lot of the physical processes and does not include important components (clouds, orography, moisture etc.), and therefore it is not expected that the idealized model could simulate accurately the projected changes. Nevertheless, the idealized model is used to understand the direct effect of the zonally symmetric temperature changes on the circulation. In the next subsections (sections 4a and 4b), the idealized model is used with the ECMWF reference to isolate the direct effect of low-latitude upper tropospheric temperature increase and Arctic amplification trends in the RCP8.5 scenario on the atmospheric circulation in the NH in the idealized GCM.

a. Upper tropospheric tropical heating using the ECMWF reference

To consider the effect of the projected low-latitude upper tropospheric temperature changes on eddy activity, the ECMWF reference temperature was modified as in Eq. (5). The simulated modified temperatures mimic the upper tropospheric tropical meridional gradient temperature changes as in an RCP8.5 scenario. As in section 3a we find that the response of the EKE and EHF in the NH is dependent on the exact details of the temperature changes [see the work of Tandon et al. (2013) and Sun et al. (2013), who show that the circulation response to tropical warming is dependent on the width of the warming]. When the meridional temperature gradient modifications are constrained to lower latitudes, the EKE and EHF amplitude tend to increase (Fig. 6, left column). When the temperature gradient increase extends deep into the subtropics, as in CMIP5 temperature projections (Fig. 1a), eddy activity decreases, and the jet tends to shift poleward (Fig. 6, right column). These results are in agreement with the conclusion of section 3 that the increase in the meridional temperature gradient and the static stability have a competing and opposite effect on the

eddy activity when the upper troposphere is warmed at lower latitudes. Specifically, the qualitative responses shown in Fig. 6 are in agreement with the results of Fig. 2.[6]

When mimicking the meridional temperature gradient RCP8.5 trends in the upper troposphere also at higher latitudes (Fig. 6, right column), the EKE response is similar to the one obtained from the RCP8.5 idealized simulation (Fig. 5) in the upper troposphere. This implies that the changes in the low-latitude upper troposphere temperature plays an important role in affecting the EKE in the upper troposphere. On the other hand, the zonal wind, EMFC, and EHF changes are significantly different from the RCP8.5 idealized simulation, indicating that temperature changes in other regions play an important role in the zonal wind and eddy fields response. Furthermore, we note that according to the results presented here, it is not clear whether the increased upper tropospheric temperature gradient (Fig. 6) will necessarily lead to increased eddy activity.

b. Arctic amplification

To consider the effect of the projected Arctic amplification on eddy activity, the ECMWF reference temperature was modified as in Eq. (6). The simulated modified temperatures mimic the lower-level meridional gradient temperature changes as in the RCP8.5 scenario. As in section 3, when the extent of the temperature gradient increases, the EKE response is shifting from a negative sign (Fig. 7e), to a mixed response (Fig. 7f, also cf. Fig. 3k). Since in the NH surface the meridional temperature gradient is constrained to relatively high latitudes (Fig. 1b), the overall response is mostly negative due to the reduction in the meridional temperature gradient, with the reduction in static stability playing a smaller role. Consequently, the qualitative circulation changes due to RCP8.5-like Arctic amplification have relatively small sensitivity to changes of the parameter ϕ_c^{Arctic} [Eq. (6)], and the two simulations presented in Fig. 7 show similar results (though their amplitude is different). The jet tends to weaken at high latitudes and increase at the jet center (Figs. 7a,b), which tends to sharpen the jet. The EHF decreases at lower levels where the gradient is reduced, indicating that the reduction in the EHF at lower levels
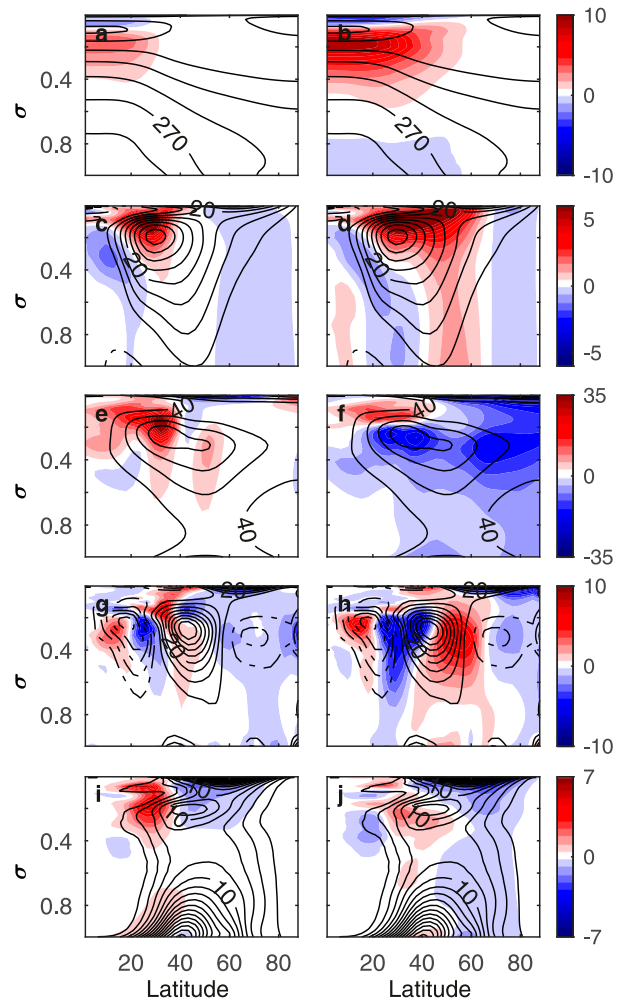

FIG. 6. The zonal wind and eddy fields response in the ECMWF reference state to low-latitude upper tropospheric meridional temperature gradient increase taken from RCP8.5 scenario. Contours show the (a),(b) temperature, (c),(d) zonal wind, (e),(f) EKE, (g),(h) EMFC $\times 10^6$, and (i),(j) EHF for the ECMWF reference temperature ($T_{\mathrm{ref}}^{\mathrm{ECMWF}}$). Colors show the difference between RCP8.5 tropical upper troposphere temperature modifications, as in Eq. (5) with parameters (left) $\phi_c^{\mathrm{tropical}} = 30°$ and (right) $\phi_c^{\mathrm{tropical}} = 60°$ and the ECMWF idealized reference. The contour intervals are 15 K (temperature), 5 m s^{-1} (zonal wind), 40 m^2 s^{-2} (EKE), 5 m s^{-2} (EMFC), and 2 K m s^{-2} (EHF). Colors have the same units as contours.

seen in the idealized RCP8.5 idealized simulation (Fig. 5e) is caused by the meridional temperature reduction at the lower levels.[7]

---

[6] Figure 6 shows only two simulations for presentation compactness reasons, but it was verified that there is a gradual change between an enhancement of the EKE and EHF for smaller values of $\phi_c^{\mathrm{tropical}}$, which is changed to a reduction in EKE and EHF for larger values of $\phi_c^{\mathrm{tropical}}$.

[7] Figure 7 shows only two simulations, but the parameter ϕ_c^{Arctic} was varied in order to investigate its effect on the eddy fields ($\phi_c^{\mathrm{Arctic}} = 30°, 35°, 40°, 45°, 50°, 55°, 60°, 65°, 70°$). Since the lower-level gradient is confined to higher latitudes and does not reach lower latitudes, the response in these simulations is qualitatively similar in these simulations, with the exception that the EKE shows an increase in a small region for lower values of ϕ_c^{Arctic} (as shown in the right column of Fig. 7).
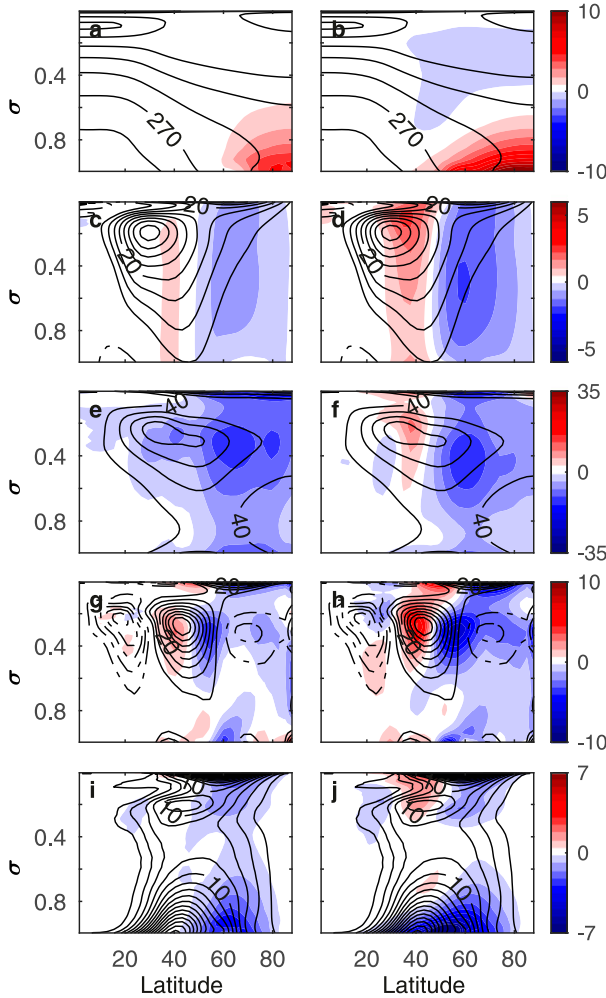
FIG. 7. The zonal wind and eddy fields response in the ECMWF reference state to polar surface meridional temperature gradient decrease taken from RCP8.5 scenario. As in Fig. 6, but for Arctic amplification simulations [Eq. (6)] with the parameters (left) $\phi_c^{\text{Arctic}} = 60°$ and (right) $\phi_c^{\text{Arctic}} = 30°$. The contour intervals are 15 K (temperature), 5 m s^{-1} (zonal wind), 50 m^2 s^{-2} (EKE), 5 m s^{-2} (EMFC), and 2 K m s^{-2} (EHF). Colors have the same units as contours.

The zonal wind, EKE, EMFC, and EHF changes due to tropical upper troposphere temperature increase and due to Arctic amplification are on the same order of magnitude. This implies that in order to understand the circulation changes in a global warming scenario that are caused by temperature modifications, it is necessary to consider both changes. This is different from the results of section 3, where the upper tropospheric changes lead to larger changes. Since both the reference and the temperature trends were not taken from a more realistic scenario in section 3, we find the results in this section more relevant when considering the effect of global warming–like temperature trends on the zonal wind and eddy fields.

c. Combined Arctic and upper tropospheric warming

In this section we investigate whether the main response in the NH in the RCP8.5 idealized simulation (Fig. 5) can be explained by these two observed temperature trends. Furthermore, it is demonstrated that the linear sum of simulations with low-latitude upper tropospheric heating and Arctic amplification gives similar eddy response as in a simulation with the combined temperature trends. The temperature modifications in the combined experiments can be expressed as

$$T_{\text{combined}}^{\text{ECMWF}} = T_{\text{ref}}^{\text{ECMWF}} + \delta T_{\text{tropical}}^{\text{ECMWF}} + \delta T_{\text{Arctic}}^{\text{ECMWF}}. \qquad (7)$$

It is found that the combined simulation (Fig. 8, middle column) and the linear sum of the separated simulation (Fig. 8, right column) give very similar results.[8] Nevertheless, small differences between the combined simulation and the linear sum of separate simulation occur in certain regions (e.g., the amplitude of the EKE changes at higher latitudes is smaller in the combined simulations). This implies that in order to understand the eddy activity changes in the idealized simulations of the combined scenario, there is no need to consider interactions between the changes caused by low-latitude upper tropospheric warming and the Arctic amplification. Furthermore, it is found that the combined simulation (Fig. 8, middle column) and the full scenario (Fig. 8, left column) simulate very similar zonal wind, EKE, and EHF changes. This implies that the two anomalous temperature trends in the low-latitude upper troposphere and the polar surface have a large effect on the circulation changes, and in the idealized simulations conducted in this study most of the zonally symmetric circulation changes are induced by these changes. Nevertheless, the combined simulation does not produce the changes in the EMFC correctly at latitudes 40°–60°N. Whereas in the idealized RCP8.5 simulation there is a weaker convergence in this region, both in the combined and in the sum of the linear simulation there is stronger convergence. Overall these results imply that in order to understand the eddy activity response due to temperature changes

---

[8] Figure 8 shows only a single combined simulation, but we verified that the qualitative results remain similar with six different parameter combinations: $\phi_c^{\text{tropical}} = 45°$, 60°, 90°, $\phi_c^{\text{Arctic}} = 30°$, 40°. These parameter choices are meant to represent the major part of the gradient changes in the polar surface and in the upper troposphere. Choosing lower (higher) values for ϕ_c^{tropical} (ϕ_c^{Arctic}) will lead to a temperature change that does not capture a major part of the gradient changes (e.g., Fig. 6a).
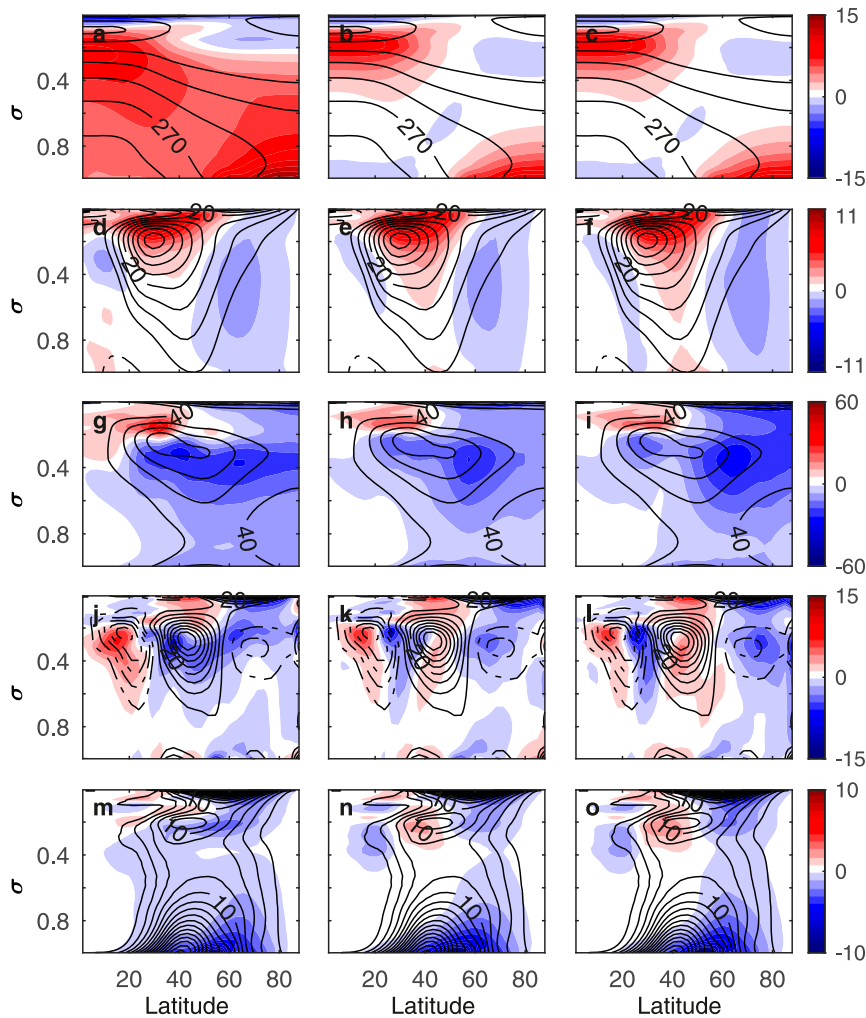
FIG. 8. Comparison between the zonal wind and eddy fields response in the ECMWF reference to (left) temperature modifications as in the RCP8.5 scenario, (middle) with combined temperature increase at the low latitudes of the upper troposphere and at the polar surface, and (right) to the response from a linear sum from separate simulations with similar temperature changes. (a)–(d) Temperature, (e)–(h) zonal wind, (i)–(l) EKE, (m)–(p) EMFC $\times$ 10^6, and (q)–(t) EHF for the (left) full RCP8.5 changes, (middle) the combined simulation [Eq. (7)] with the parameters $\phi_c^{\text{tropical}} = 60°$ and $\phi_c^{\text{Arctic}} = 30°$, and (right) the linear sum of a simulation upper tropospheric tropical temperature increase ($\phi_c^{\text{tropical}} = 60°$) and Arctic amplification ($\phi_c^{\text{Arctic}} = 30°$). The contour intervals are 15 K (temperature), 5 m s^{-1} (zonal wind), 40 m^2 s^{-2} (EKE), 5 m s^{-2} (EMFC), and 2 K m s^{-2} (EHF). Colors have same units as contours.

as in the RCP8.5 scenario, it is enough to consider the low-latitude upper tropospheric temperature increase and the Arctic amplifications, though there are some exceptions when it is not enough to consider these changes (changes in the EMFC).

5. Conclusions

In this study, the zonal wind and eddy fields response to global warming–like temperature variations are investigated using an idealized GCM with a modified

Newtonian cooling scheme. The modified Newtonian cooling scheme enables simulation of any chosen zonal mean temperature distribution. This allows us to systematically study how temperature changes in different regions and with different spatial structures affect the circulation. Many different studies have used idealized GCMs to investigate the circulation response to global warming–like heating profiles (e.g., Polvani and Kushner 2002; Kushner and Polvani 2004; Lorenz and DeWeaver 2007; Lim and Simmonds 2009; Butler et al. 2010; Lu et al. 2014). One limitation of these studies is

that they prescribe a diabatic heating profile that resembles the projected temperature changes. For example, to study the effect of Arctic amplification on the circulation, heating at the polar surface is prescribed (Butler et al. 2010). However, inducing diabatic warming at a certain region may lead to temperature changes also in other regions due to temperature advection, and the resulting circulation will be affected by temperature changes in regions that were not intended to be modified. The method used in this study allows the investigation of the zonal mean wind and eddy fields response to global warming–like temperature trends.

The zonal wind and eddy fields responses to low-latitude upper tropospheric and polar surface temperature increase are investigated. It is found that the response to low-latitude upper tropospheric temperature increase and to polar surface temperature increase is dependent on the shape of the temperature changes (Figs. 2 and 3). Specifically, it is found that the latitudinal extent of these temperature changes has a large effect on the response of eddy fields. For example, it is shown that as the low-latitude upper tropospheric temperature increase penetrates deeper into midlatitudes, the responses of the EKE and EHF tend to shift from an increase to a decrease (Fig. 2). Similarly, it is found that when the high-latitude surface warming is extended toward the tropics, the response of the EKE changes from a decrease to an increase. These results are explained by the interplay between the meridional temperature gradient and the static stability. When the meridional temperature gradient is modified only at certain vertical levels, the Brunt–Väisälä frequency also changes (e.g., Figs. 1b,c and Fig. A1). Therefore, when the low-latitude upper troposphere is anomalously warmed, the meridional temperature gradient is increased, but at the same time the dry static stability increases. These two trends have an opposite effect on baroclinicity. Similarly, when the surface is warmed at high latitudes, the meridional temperature gradient decreases, but at the same time also the static stability decreases. When the latitudinal extent of the temperature changes increases (while keeping the meridional temperature gradient magnitude constant), the static stability tends to play a larger role since it is modified in a broader region (section 3 and appendix A). It is demonstrated that in order to understand the circulation response to global warming–like temperature changes, both the static stability changes and meridional temperature gradient need to be taken into account, and considering only the meridional temperature gradient changes is not sufficient to understand the circulation changes (section 3 and appendixes B and C).

As shown in this study, it is not trivial to determine whether the temperature gradient or the static stability changes affect more the eddy fields (e.g., Fig. 2). Hence,

studies that considered only changes in the meridional temperature gradient might not be sufficient to give an indication whether the low-latitude upper troposphere warming or the Arctic amplification will have a larger effect on the circulation [e.g., Held and O'Brien (1992) used a three-layer quasigeostrophic model, and considered only a meridional temperature gradient modifications, while static stability was unchanged]. To put the topic of eddy sensitivity to upper or lower baroclinicity changes in the context of global warming, it is necessary to simulate temperature changes that are representing global warming projections and affect both the meridional temperature gradient and static stability.

Highlighting the importance of static stability changes in affecting the circulation in a global warming scenario, and focusing simultaneously on changes in the meridional temperature gradient and in the static stability, could shed light on the results of Lunkeit et al. (1998) and Yuval and Kaspi (2016). Lunkeit et al. (1998) used an idealized model with realistic temperature profiles to investigate the effects of global warming on atmospheric circulation. Lunkeit et al. (1998) modified the temperature field at the lower and upper levels separately, using the difference between the historical temperature field and a global warming scenario. They found that when only the lower levels are modified (decreasing the temperature gradient), eddy activity increases, and when only the upper levels are modified (increasing the temperature gradient), eddy activity decreases (see Fig. 9 in their paper). Lunkeit et al. (1998) found this result surprising, and explained their results by the domination of the local modes over the global modes (Pierrehumbert 1984). As shown here, a simpler interpretation to their results is that the static stability decreases (increases) when the temperature is increased only at the lower (upper) levels. Also, the results of Yuval and Kaspi (2016), which showed that eddy activity changes much more when the upper-level temperature gradient is modified compared to the lower-level temperature gradient, can be partly explained by the static stability changes. In those simulations the temperature gradient was modified by changing the temperature at higher latitudes and at different vertical levels. Therefore, modifying the temperature gradient at lower levels led to opposite effects of the meridional temperature gradient and static stability on baroclinicity (as in the case of Arctic amplification). Conversely, modifying the temperature in the upper levels led to static stability changes and meridional temperature gradient changes that both tended to increase or decrease the baroclinicity in the same direction. This observation could explain the larger changes in eddy fields when the upper levels were modified compared to the small response when the lower levels were modified. Furthermore, similarly to Lunkeit et al. (1998),

Yuval and Kaspi's (2016) simulations showed a decrease in eddy activity when the meridional temperature gradient was increased at the lower levels, which can be explained by an increase in the static stability.

Two different reference states are used in this study. One is taken from the Held and Suarez (1994) reference temperature, and the second is taken from the ECMWF reanalysis data (section 2). Using the Held and Suarez (1994) reference temperature with imposed prescribed temperatures modifications [Eqs. (2) and (3)] at low-latitude upper troposphere and polar surface, it is found that the eddy activity response is dominated by the tropical upper troposphere (section 3c). To investigate the effect of global warming–like temperature changes on the circulation in a more realistic reference state, the zonally mean DJF temperature taken from ECMWF data ($T_{\mathrm{ref}}^{\mathrm{ECMWF}}$) is simulated. The use of a second reference state, which resembles Earth's temperature and circulation (especially in the NH; see Fig. C2 in section b of appendix C), is necessary since different reference states have different circulation response when the same temperature changes are applied. For example, when the RCP8.5 temperature changes are imposed on the ECMWF reference state (Fig. 5), the response is different compared to the same changes imposed on the Held and Suarez (1994) reference state (Fig. C2).[9] This result has broader implications, and it suggests that idealized studies should use several representing reference states to verify the robustness of the results.

The ECMWF reference is used to study the effect of RCP8.5 temperature trends in the NH winter on zonal wind and eddy activity. The RCP8.5 temperature gradient changes are imposed on the ECMWF reference at the low-latitude upper troposphere [Eq. (5)] and at the Arctic surface [Eq. (6)] separately (Figs. 6 and 7). Similarly to what is found using the Held and Suarez (1994) reference, it is found that the meridional temperature gradient latitudinal extent have a large effect on the circulation in these simulations. Furthermore, we find that gradient changes in both regions have a large effect on eddy fields (right columns in Figs. 6 and 7). For example, while the EKE changes are larger when the upper troposphere gradient is modified, the EHF changes are larger when the polar surface is warmed (right columns in Figs. 6 and 7). It is found that the low-latitude upper tropospheric temperature gradient and the Arctic amplification have an opposite effect (and with similar magnitude) on EMFC. The low-latitude upper

tropospheric temperature gradient tends to shift poleward the EMFC (and the zonal wind, Figs. 6d and 6h), while the Arctic amplification has an opposite effect (Fig. 7h). This implies that the poleward shift of the storm tracks in the NH might have a large variability between models because of the competing effects of the two temperature trends (and the large variability in the polar amplification), whereas in the SH the poleward shift is more robust because there is no anomalous warming in Antarctica.

We find that the linear sum of simulations with upper tropospheric tropical heating and Arctic amplification gives very similar eddy response as in a single simulation with the combined (tropical upper troposphere and Arctic) temperature trends (Fig. 8). This implies that there is little interaction between the circulation changes due to the temperature changes in the tropical upper troposphere and polar surface in the idealized GCM. Furthermore, comparing the zonal wind and eddy fields response in the combined simulation to the full idealized RCP8.5 (where temperature trends are as in the RCP8.5 in all regions), we find that in most regions the zonal wind and eddy fields have similar changes and there is agreement between the two simulations. This implies that the temperature trends at the tropical upper troposphere and at the Arctic are the cause of most of the circulation changes in the idealized model when considering a global warming scenario (Fig. 8).

APPENDIX A

Changes in the Meridional Temperature Gradient and Static Stability When the Tropical Upper Troposphere Temperature Increases

Low-latitude upper tropospheric increases in temperatures (as in Fig. 2) lead to an increase in the meridional temperature gradient (Figs. A1e–h) and an increase in the Brunt–Väisälä frequency at the troposphere (Figs. A1i–l). These changes have opposite effect on baroclinicity. In Figs. A1m–p the changes in Eady growth rate are plotted, where the Eady growth rate is calculated as $0.31 g \partial_y T/(NT)$ (where g is gravitational acceleration and N is the Brunt–Väisälä frequency).

---

[9] The major differences are found in the SH, but some differences are found also in the NH (e.g., jet and surface wind shift does not occur in the ECMWF reference).
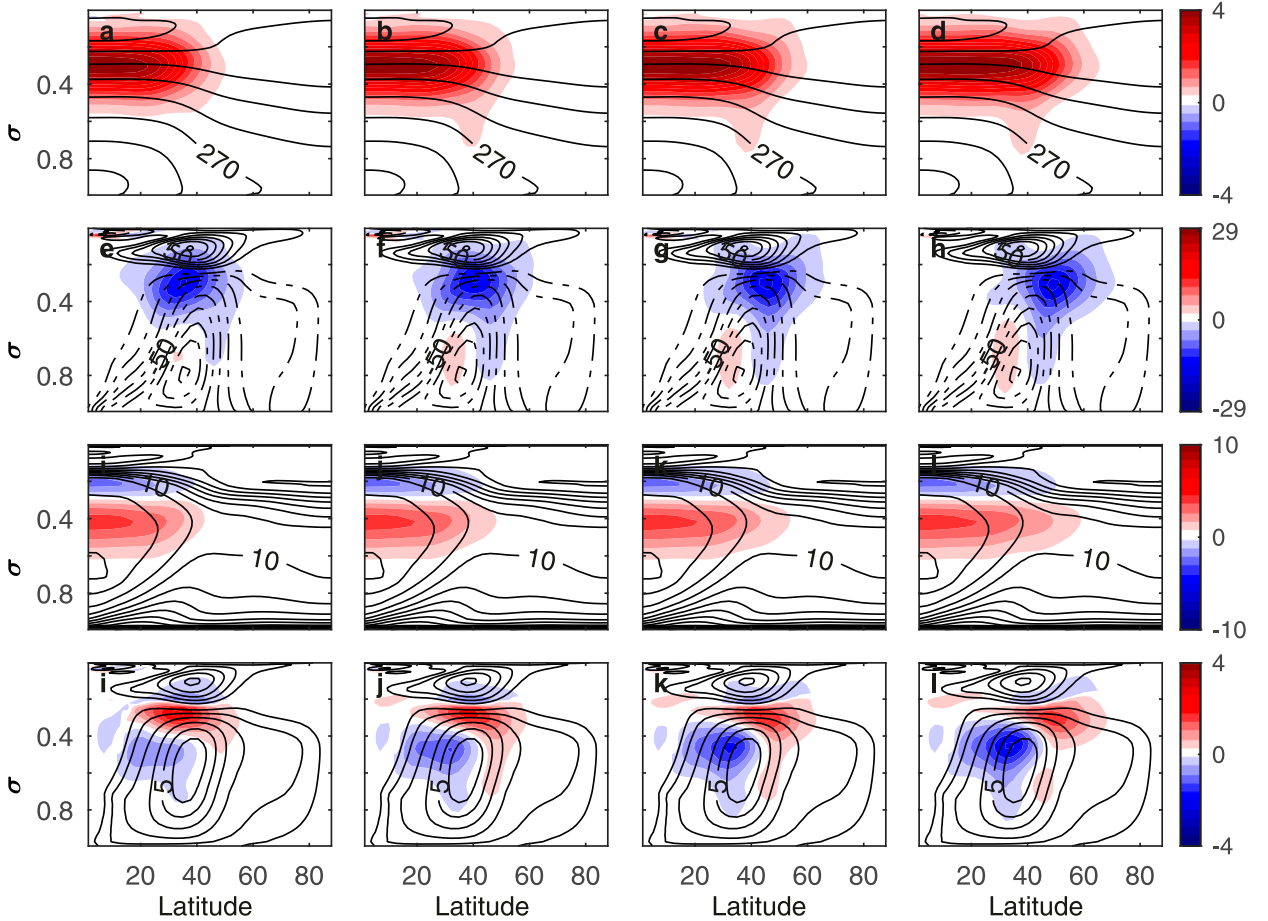
FIG. A1. The changes in meridional temperature gradient and in the Brunt–Väisälä frequency due to low-latitude upper tropospheric temperature increase with different latitudinal extent. (a)–(d) Temperature, (e)–(h) meridional temperature gradient, (i)–(l) Brunt–Väisälä frequency, and (m)–(p) the Eady growth rate for simulations where the upper troposphere was modified with tropical upper tropospheric temperature increase as in Eq. (2); the parameters $A = 2K$, $\phi_c = 35°$, $40°$, $45°$, $50°$, $\phi_w = 10°$, $\sigma_c = 0.3$, and $\sigma_w = 0.11$. Colors indicate the deviation from the reference simulation and contours show the reference simulation fields. The contour intervals are 15 K (temperature), $10\,\mathrm{K\,m^{-1}} \times 10^{-7}$ (meridional temperature gradient), $2\,\mathrm{s^{-1}} \times 10^{-3}$ (Brunt–Väisälä frequency), and $1\,\mathrm{s^{-1}} \times 10^{-6}$ (Eady growth rate). Colors have the same units as contours.

Furthermore, when the meridional extent of the temperature modification in Eq. (2) is increased (larger ϕ_c^{upper}), the meridional temperature gradient shifts poleward, but its magnitude is unchanged (Figs. A1e–h). Conversely, when the meridional extent of the temperature modification is increased, the Brunt–Väisälä frequency changes span over a larger region (Figs. A1i–l), and therefore these changes have a larger effect on the circulation as the parameter ϕ_c^{upper} is increased (see discussion in section 3). This result can also be seen in Figs. A1m–p, where the Eady growth rate tend to be overall more negative as the width of the temperature changes is broadened. Hence, it is expected that when the extent of the temperature changes is larger, the static stability plays a larger role and tends to weaken the eddy fields.

APPENDIX B

Highlighting the Interplay between Static Stability Changes and Meridional Temperature Gradient Changes

a. Upper tropospheric meridional temperature gradient changes by cooling at high latitudes

To investigate the importance of the static stability changes when the upper tropospheric meridional temperature gradient changes on eddy activity, and better understand the interplay between the effects of static stability and meridional temperature gradient changes on eddy activity, additional simulations were conducted. These simulations have a similar meridional temperature gradient changes as described in Eq. (2), but have
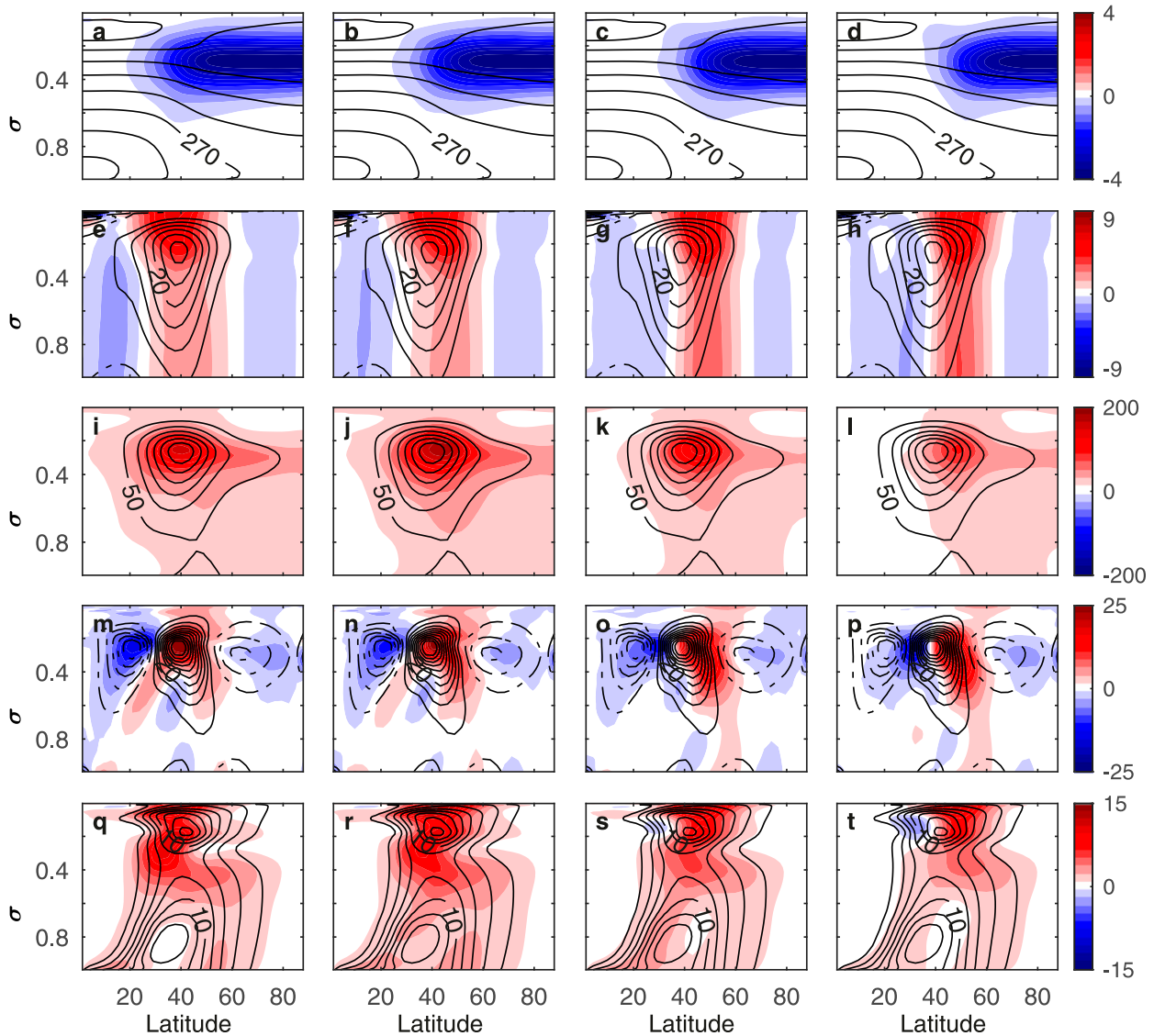
FIG. B1. The zonal wind and eddy fields response to increased meridional temperature gradient in the upper tropospheric due to high-latitude cooling in an idealized GCM. As in Fig. 2, but for polar upper troposphere warming. The meridional temperature gradient in these simulations is similar to the gradients of the simulations presented in Fig. 2, but the static stability modifications have opposite sign and are located in different regions. The contour intervals are 15 K (temperature), 5 m s^{-1} (zonal wind), 50 m^2 s^{-2} (EKE), 5 m s^{-2} (EMFC), and 2 K m s^{-2} (EHF). Colors have the same units as contours.

different static stability changes. In these simulations the temperature field was modified as follows:

$$\delta T_{\text{tropical−inverse}}(0 \leq \phi \leq \phi_c^{\text{upper}}) = \int_{0°}^{\phi} \partial_{\phi_i} \delta T_{\text{tropical}} \, d\phi_i$$

(B1)

and $\delta T_{\text{tropical−inverse}}(\phi < 0) = \delta T_{\text{tropical−inverse}}(\phi > 0)$. These simulations have decreased temperatures at the upper levels of higher latitudes (Figs. B1a–d), leading to an overall increase in baroclinicity, due to both a decrease in the static stability and an increase in the

meridional temperature gradient. Equations (2) and (B1) have identical meridional temperature gradient changes, but different static stability changes.

Both the EKE and EHF increases in the simulations with upper tropospheric cooling at high latitudes (Fig. B1), and with significantly larger amplitude compared to upper tropospheric low-latitude heating simulations (Fig. 2). Furthermore, the EMFC is intensified (larger convergence in converging regions and vice versa), leading to a general intensification of the jet stream, rather than a shift in the two left panels of Fig. B1. In the two right panels, the static stability and meridional temperature gradient are
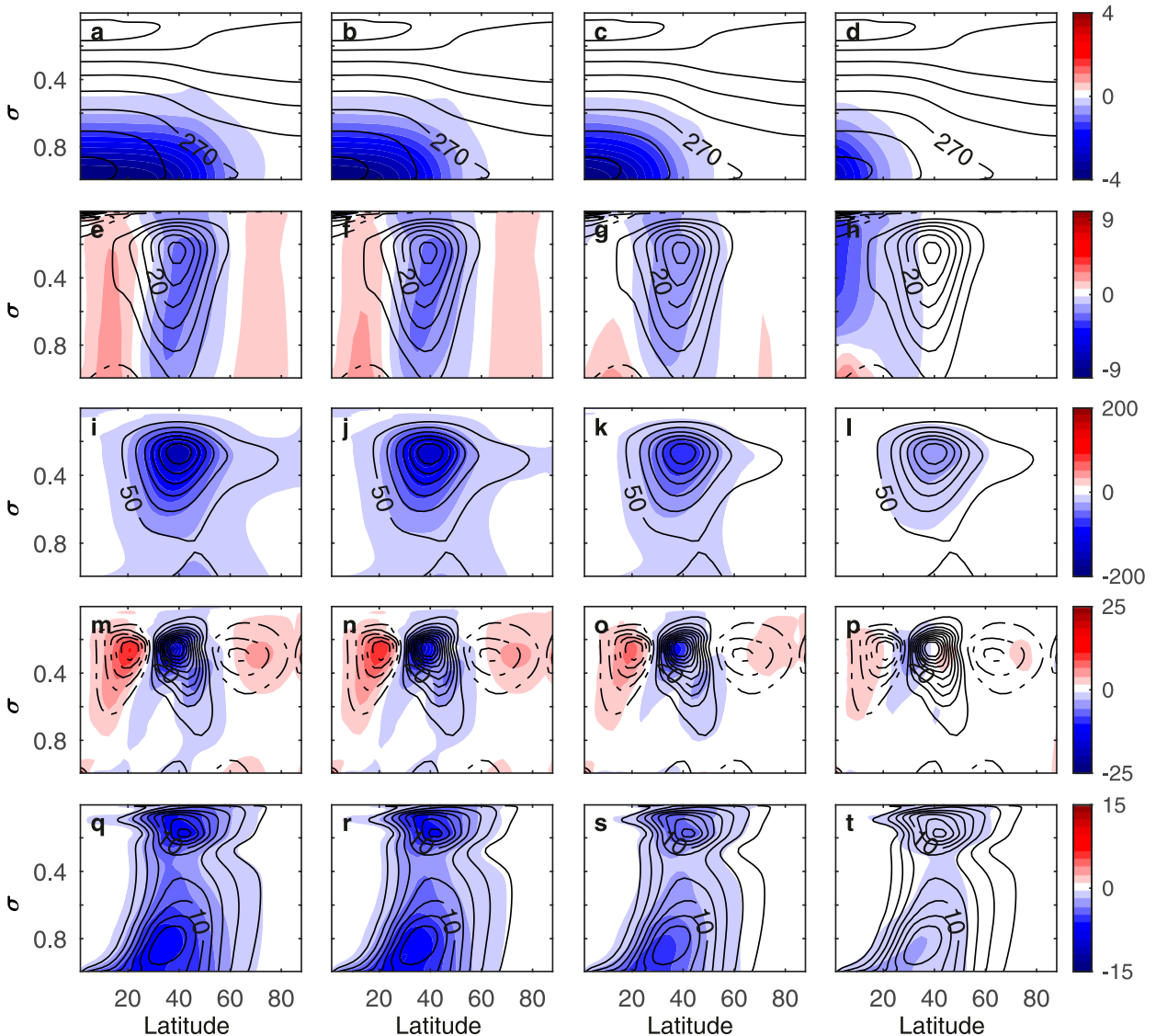
FIG. B2. The zonal wind and eddy fields response to decreased meridional temperature gradient at the surface due to low-latitude cooling in idealized GCM. As in Fig. 3, but for lower troposphere cooling at the lower latitudes. The meridional temperature gradient in these simulations is similar to the gradients of the simulations presented in Fig. 3, but the static stability modifications have opposite sign and are located in different regions. The contour intervals are 15 K (temperature), 5 m s^{-1} (zonal wind), 50 m^2 s^{-2} (EKE), 5 m s^{-2} (EMFC), and 2 K m s^{-2} (EHF). Colors have the same units as contours.

modified at higher latitudes, and have a smaller effect on eddy activity compared to the two left panels. Consequently, the EKE response is weaker, and there is a jet shift (partly due to the high-latitude increase in temperature gradient). The large eddy response, as well as the different zonal wind response, emphasize that changing the meridional temperature gradient at the upper troposphere, as a result of high-latitude upper-level temperature reduction as in Fig. B1 or as a result of upper-level low-latitude warming as in Fig. 2, leads to a very different circulation response. Since the meridional temperature gradient is identical in the two

scenarios, we conclude that these large differences in the response are due to the different changes in static stability. We note that the qualitative results are obtained also for other parameter choices ($\sigma_c^{upper} = 0.2$, 0.3, 0.4 were simulated with a gradual change in ϕ_c^{lower}).

b. Lower-level meridional temperature gradient changes by cooling at low latitudes

To investigate the importance of the static stability changes when the meridional temperature gradient changes in the lower levels, 48 additional simulations

were conducted. These simulations have a similar meridional gradient change as described in Eq. (3), but have different static stability changes. In these simulations the temperature field was modified as follows:

$$\delta T_{\text{arctic–inverse}}(\phi_c^{\text{lower}} \leq \phi \leq 90°) = -\int_\phi^{90°} \partial_{\phi_i} \delta T_{\text{arctic}} \, d\phi_i$$

$$\text{(B2)}$$

and $\delta T_{\text{arctic–inverse}}(\phi < 0) = \delta T_{\text{arctic–inverse}}(\phi > 0)$. These simulations have decreased temperatures at lower latitudes close to the surface (Figs. B2a–d), leading to an overall increase in atmospheric stability, both due to an increase in the static stability and a decrease in the meridional temperature gradient.

Both the EKE and EHF decreases in the simulations with lower-latitude surface cooling, and with significantly larger amplitude compared to upper tropospheric tropical heating simulations (cf. Fig. B2 to Fig. 3). Since the meridional temperature gradient was identical in the two scenarios, we conclude that these large differences in the response of eddy fields are due to the different changes in static stability. We note that the qualitative results are obtained also for other parameter choices (all the combinations of $\phi_w^{\text{lower}} = 10°$, $20°$, $30°$ and $\sigma_w^{\text{lower}} = 0.1$, 0.2 were simulated with a gradual change in ϕ_c^{lower}).

APPENDIX C

Reference State Differences and Their Different Responses to Global Warming Temperature Projections

a. Response of the Held–Suarez reference to RCP8.5 temperature changes

To show that the eddy response to temperature changes is dependent on the chosen reference when considering global warming–like temperature changes, the Held and Suarez (1994) reference temperature ($T_{\text{ref}}^{\text{HS}}$) was modified as follows:

$$T_{\text{HS–RCP}} = T_{\text{ref}}^{\text{HS}} + T_{\text{RCP85}}^{\text{mod}}. \quad \text{(C1)}$$

These temperature changes are similar to the temperature changes considered in Fig. 5, where the projected changes from the RCP8.5 scenario were added to the ECMWF reference. The circulation responses to these changes are plotted in Fig. C1. There are large differences in the eddy field response when the temperature is modified as in the RCP8.5 scenario, but with two different
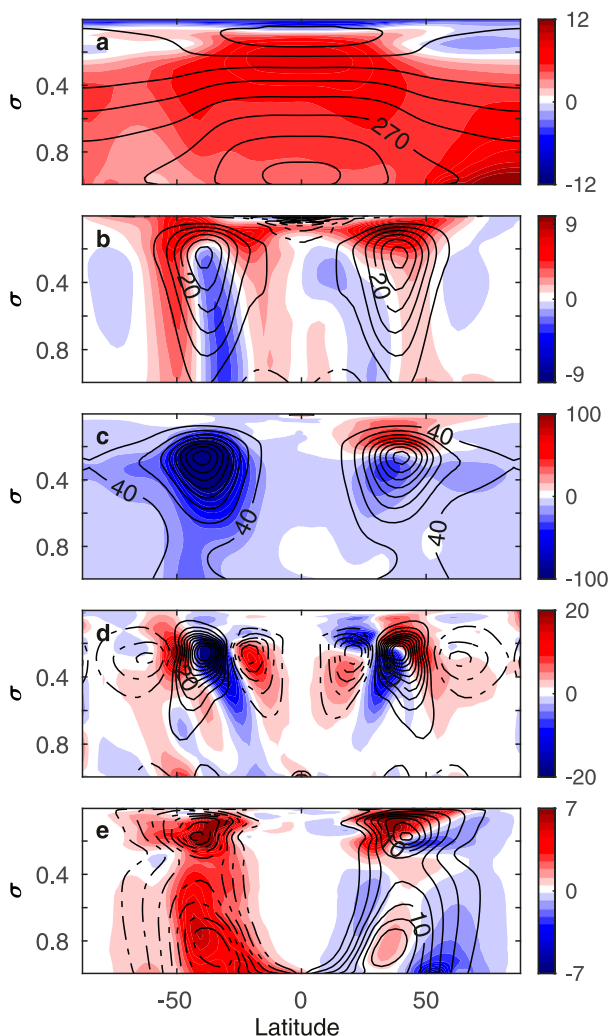

FIG. C1. The zonal wind and eddy fields response in the Held and Suarez (1994) reference state to temperature projections taken from RCP8.5 scenario. As in Fig. 5, but with the Held and Suarez (1994) reference temperature.

reference states. For example, the EKE response in the SH has an opposite sign where EKE peaks (cf. Fig. C1 and Fig. 5). Furthermore, the EMFC in the NH and the EHF in the SH have an opposite response in the two simulations in most regions. This implies that in order to investigate the circulation response to global warming–like temperature changes, we need to consider a reference state that is as realistic as possible. Therefore, in section 4 we consider a reference state whose temperature field is taken from reanalysis data. The fact that two different idealized reference states that represent Earth-like circulation have a different response to the same temperature modifications implies that idealized studies should use several representing reference states to verify the robustness of the results.
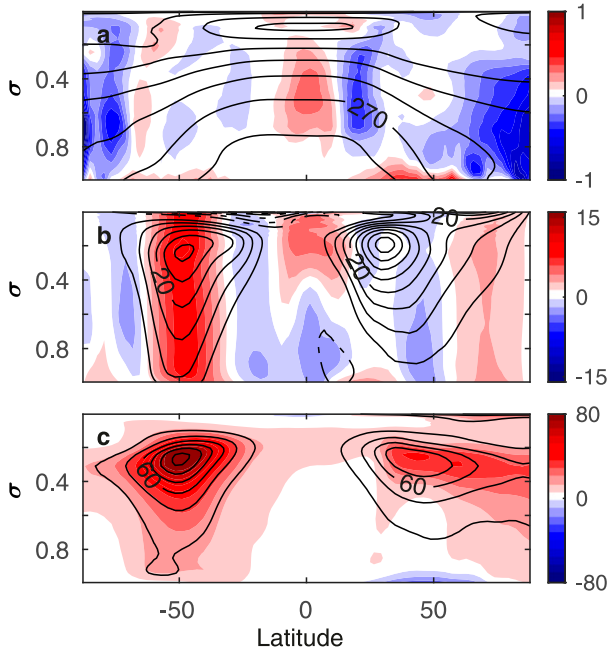
FIG. C2. Comparison between the ECMWF reanalysis data and the zonally symmetric ECMWF reference simulation. Contours show the zonally averaged wintertime ECMWF reanalysis data for the (a) temperature (contour intervals 15 K), (b) zonal wind (contour intervals 5 m s^{-1}), and (c) EKE (is calculated using a Butterworth bandpass filter with a cutoff period of 3–10 days; contour intervals 20 m^2 s^{-2}). Colors show the difference between the ECMWF reanalysis data and the ECMWF reference described in section 2c.
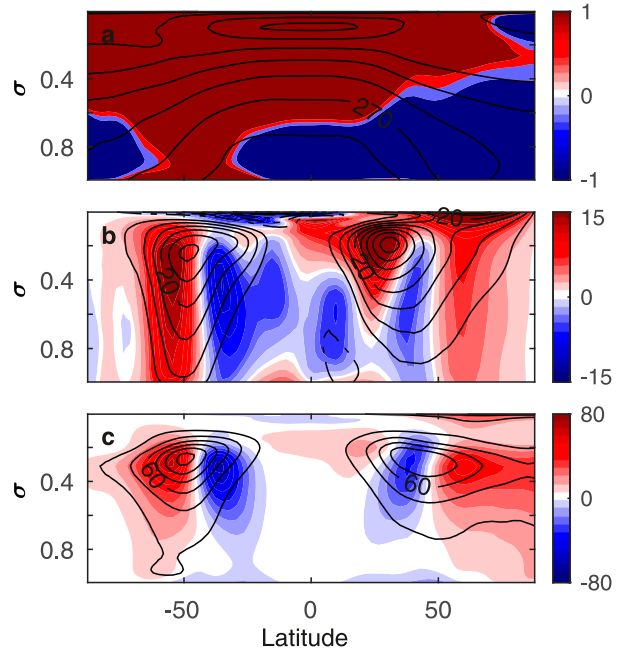

FIG. C3. Comparison between the ECMWF reanalysis data and the Held and Suarez (1994) reference simulation. Contours show the zonally averaged wintertime ECMWF reanalysis data for the (a) temperature (contour intervals 15 K), (b) zonal wind (contour intervals 5 m s^{-1}), and (c) EKE (calculated using a Butterworth bandpass filter with a cutoff period of 3–10 days; contour intervals 20 m^2 s^{-2}). Colors show the difference between the ECMWF reanalysis data and the Held and Suarez (1994) reference.

b. ECMWF reanalysis data versus zonally symmetric reference simulations

In this appendix, the differences between the ECMWF reanalysis data and the zonally symmetric reference simulations used in this study are discussed. To compare the EKE results of the simulations to the reanalysis data, the EKE is calculated using a Butterworth bandpass filter with a cutoff period of 3–10 days, both for the reanalysis data and the simulations (therefore, the EKE of the reference simulations is different from the other figures that calculated EKE as the deviation from the zonal and time mean). Figure C2 shows the temperature, zonal wind, and EKE differences between the ECMWF reanalysis data and the ECMWF zonally symmetric idealized reference simulation described in section 2c. The temperature differences are smaller than 1 K, indicating that the Newtonian relaxation scheme that is used in this study is able to reproduce the target temperature (Fig. C2a). The zonal wind differences are very large in the SH and are much smaller in the NH (on the order of 2 m s^{-1}; Fig. C2b). The wind differences are mostly barotropic, which implies

that the wind differences are mostly due to differences in the EMFC, leading to large differences in the surface winds. Furthermore, the EKE in the SH is much weaker in the simulation (Fig. C2c), whereas in the NH the EKE differences are smaller, but still significant (up to 40% differences in the NH). Figure C2 shows the differences between the ECMWF reanalysis data and the Held and Suarez (1994) reference simulation. The differences in the surface winds and EKE are larger than the differences shown in Fig. C2 for the NH. Therefore, although there are significant differences between the ECMWF reanalysis data and idealized ECMWF simulation, we find the idealized zonally symmetric ECMWF reference to be more suitable than the Held and Suarez (1994) for this study.

We note that we do not expect to reproduce the ECMWF eddy fields for several reasons. First, the simulations in this study are zonally symmetric and do not include orography, ocean, or moisture, which play an important role in setting the eddy fields. For example, Chang (2006) argues that eddies are weaker in such idealized simulations because of the use of dry static stability and not the moist static stability. Second, the model we use is not tuned in any way to reproduce the
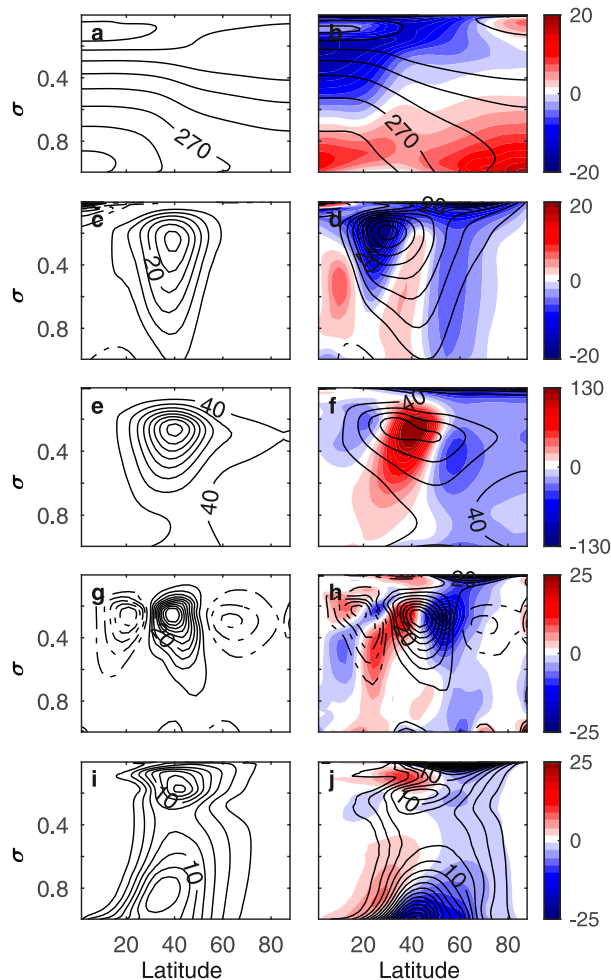
FIG. C4. Comparison between the Held and Suarez (1994) reference simulation and the ECMWF reference simulation. Contours show values for (left) the Held and Suarez (1994) reference simulation, and (right) the ECMWF reference for the (a),(b) temperature (contour intervals 15 K), (c),(d) zonal wind (contour intervals $5 \, \text{m s}^{-1}$, (e),(f) EKE (contour intervals $40 \, \text{m}^2 \, \text{s}^{-2}$), (g),(h) EMFC (contour intervals $5 \, \text{m s}^{-2}$), and (i),(j) EHF (contour intervals $2 \, \text{K m s}^{-2}$). Colors on the right panels show the difference between the Held and Suarez (1994) reference and the idealized ECMWF reference simulation described in section 2c.

eddy fields, and different parameters except the relaxation temperature could affect the eddy fields magnitude (e.g., the relaxation time). The small EKE that is obtained in the simulation in the SH implies that the missing model components are important to excite eddies during the summer of the SH. In an idealized GCM simulations, where the diabatic heating was prescribed to obtain a zonally asymmetric DJF reanalysis data (Chang 2006) and orography was included, the eddies in the summer hemisphere were not negligible, indicating that zonal asymmetries might play a large role in exciting eddies during summer.

c. Comparison between the HS94 and ECMWF idealized reference states in the NH

Figure C3 shows the differences between the Held and Suarez (1994) and ECMWF (where the relaxation temperature is $T_{\text{ref}}^{\text{ECMWF}}$) reference simulations. The figure shows that although there are some similarities between the two references (e.g., jets and EMFC have similar shapes), there are large-amplitude differences in all fields, as well as differences in the position of different fields [e.g., the surface winds and EMFC are shifted equatorward in Held and Suarez (1994)]. Differences between reference states in the location of large-scale circulation patterns, such as the jet stream, could potentially lead to different circulation response to thermal forcing.

APPENDIX D

Potential Drawbacks of the Fast Zonal Relaxation Method

The main difference between the Newtonian relaxation method that was used in this study and other Newtonian relaxation methods is that the relaxation time of the zonal mean and the eddies are on very different time scales. The zonal mean relaxation time scale is 100 times faster. This allows a relatively accurate reproduction of a prescribed (zonally mean) temperature distribution.

The main clear caveat of this method is the short relaxation time of the mean state. This short time scale could potentially interfere with the eddy life cycle at the stage when eddies act to change the mean fields, and consequently eddies would have different magnitudes owing to the strong zonal-mean relaxation. However, in appendix B of Yuval and Kaspi (2017) it is shown that different simulations that have similar temperature distribution, where in each simulation there is a different relaxation time for the zonally mean temperature, have almost identical eddy field response to changes in the temperature field. That is, zonally symmetric simulations with more similar relaxation time for the eddy and mean temperature field and simulations with the fast zonal mean relaxation (which was used in this study) show almost identical eddy field response to changes in the temperature field.

The main difference between a slower (and more "realistic") relaxation time for the zonally mean state and the method with a fast zonal relaxation that is used in this study is that in a slower relaxation time simulations the zonal mean temperature can deviate from the time mean. Conversely, in the method used in this study, the zonal mean temperature is (approximately) constrained at every time

instance to the time mean. The results presented in appendix B of Yuval and Kaspi (2017) (similar eddy field changes in both methods) imply that the contribution of the deviation of the zonal mean from its time mean does not contribute significantly to the eddies in these simulations.

A main advantage in using the method used in this study is that it requires less computation time since the computation of the relaxation matrix is trivial (it is just the target temperature). This allowed us to perform large number of simulations and verify the robustness of our results using many different configurations and different parameters.

REFERENCES

Bengtsson, L., and K. I. Hodges, 2006: Storm tracks and climate change. *J. Climate*, **19**, 3518–3543, https://doi.org/10.1175/JCLI3815.1.

Bintanja, R., R. G. Graversen, and W. Hazeleger, 2011: Arctic winter warming amplified by the thermal inversion and consequent low infrared cooling to space. *Nat. Geosci.*, **4**, 758–761, https://doi.org/10.1038/ngeo1285.

Butler, A. H., D. W. J. Thompson, and R. Heikes, 2010: The steady-state atmospheric circulation response to climate change–like thermal forcings in a simple general circulation model. *J. Climate*, **23**, 3474–3496, https://doi.org/10.1175/2010JCLI3228.1.

Cai, M., 2005: Dynamical amplification of polar warming. *Geophys. Res. Lett.*, **32**, L22710, https://doi.org/10.1029/2005GL024481.

——, 2006: Dynamical greenhouse-plus feedback and polar warming amplification. Part I: A dry radiative-transportive climate model. *Climate Dyn.*, **26**, 661–675, https://doi.org/10.1007/s00382-005-0104-6.

Chang, E. K. M., 2006: An idealized nonlinear model of the Northern Hemisphere winter storm tracks. *J. Atmos. Sci.*, **63**, 1818–1839, https://doi.org/10.1175/JAS3726.1.

——, S. Lee, and K. L. Swanson, 2002: Storm track dynamics. *J. Climate*, **15**, 2163–2183, https://doi.org/10.1175/1520-0442(2002)015<02163:STD>2.0.CO;2.

——, Y. Gou, and X. Xia, 2012: CMIP5 multimodel ensemble projection of storm track change under global warming. *J. Geophys. Res.*, **117**, D23118, https://doi.org/10.1029/2012JD018578.

Chen, G., J. Lu, and D. M. W. Frierson, 2008: Phase speed spectra and the latitude of surface westerlies: Interannual variability and global warming trend. *J. Climate*, **21**, 5942–5959, https://doi.org/10.1175/2008JCLI2306.1.

Dee, D. P., and Coauthors, 2011: The ERA-Interim reanalysis: Configuration and performance of the data assimilation system. *Quart. J. Roy. Meteor. Soc.*, **137**, 553–597, https://doi.org/10.1002/qj.828.

Eady, E. T., 1949: Long waves and cyclonic waves. *Tellus*, **1**, 33–52, https://doi.org/10.3402/tellusa.v1i3.8507.

Hall, N. M. J., B. J. Hoskins, P. J. Valdes, and C. A. Senior, 1994: Storm tracks in a high-resolution GCM with doubled carbon dioxide. *Quart. J. Roy. Meteor. Soc.*, **120**, 1209–1230, https://doi.org/10.1002/qj.49712051905.

Held, I. M., 1993: Large-scale dynamics and global warming. *Bull. Amer. Meteor. Soc.*, **74**, 228–242, https://doi.org/10.1175/1520-0477(1993)074<0228:LSDAGW>2.0.CO;2.

——, and E. O'Brien, 1992: Quasigeostrophic turbulence in a three-layer model: Effects of vertical structure in the mean shear. *J. Atmos. Sci.*, **49**, 1861–1870, https://doi.org/10.1175/1520-0469(1992)049<1861:QTIATL>2.0.CO;2.

——, and M. J. Suarez, 1994: A proposal for the intercomparison of the dynamical cores of atmospheric general circulation models. *Bull. Amer. Meteor. Soc.*, **75**, 1825–1830, https://doi.org/10.1175/1520-0477(1994)075<1825:APFTIO>2.0.CO;2.

Kidston, J., G. Vallis, S. Dean, and J. Renwick, 2011: Can the increase in the eddy length scale under global warming cause the poleward shift of the jet streams? *J. Climate*, **24**, 3764–3780, https://doi.org/10.1175/2010JCLI3738.1.

Kushner, P. J., and L. M. Polvani, 2004: Stratosphere–troposphere coupling in a relatively simple AGCM: The role of eddies. *J. Climate*, **17**, 629–639, https://doi.org/10.1175/1520-0442(2004)017<0629:SCIARS>2.0.CO;2.

Li, Y., D. W. J. Thompson, S. Bony, and T. M. Merlis, 2019: Thermodynamic control on the poleward shift of the extratropical jet in climate change simulations: The role of rising high clouds and their radiative effects. *J. Climate*, **32**, 917–934, https://doi.org/10.1175/JCLI-D-18-0417.1.

Lim, E.-P., and I. Simmonds, 2009: Effect of tropospheric temperature change on the zonal mean circulation and SH winter extratropical cyclones. *Climate Dyn.*, **33**, 19–32, https://doi.org/10.1007/s00382-008-0444-0.

Liu, J., J. A. Curry, H. Wang, M. Song, and R. M. Horton, 2012: Impact of declining Arctic sea ice on winter snowfall. *Proc. Natl. Acad. Sci. USA*, **109**, 4074–4079, https://doi.org/10.1073/pnas.1114910109.

Lorenz, D. J., 2014: Understanding midlatitude jet variability and change using Rossby wave chromatography: Wave–mean flow interaction. *J. Atmos. Sci.*, **71**, 3684–3705, https://doi.org/10.1175/JAS-D-13-0201.1.

——, and E. T. DeWeaver, 2007: Tropopause height and zonal wind response to global warming in the IPCC scenario integrations. *J. Geophys. Res.*, **112**, D10119, https://doi.org/10.1029/2006JD008087.

Lu, J., G. Chen, and D. M. Frierson, 2008: Response of the zonal mean atmospheric circulation to El Niño versus global warming. *J. Climate*, **21**, 5835–5851, https://doi.org/10.1175/2008JCLI2200.1.

——, L. Sun, Y. Wu, and G. Chen, 2014: The role of subtropical irreversible PV mixing in the zonal mean circulation response to global warming–like thermal forcing. *J. Climate*, **27**, 2297–2316, https://doi.org/10.1175/JCLI-D-13-00372.1.

Lunkeit, F., L. Fraedrich, and S. E. Bauer, 1998: Storm tracks in warmer climate: Sensitivity studies with a simplified global circulation model. *Climate Dyn.*, **14**, 813–826, https://doi.org/10.1007/s003820050257.

Manabe, S., and R. J. Stouffer, 1980: Sensitivity of a global climate model to an increase of CO_2 concentration in the atmosphere. *J. Geophys. Res.*, **85**, 5529–5554, https://doi.org/10.1029/JC085iC10p05529.

——, and R. T. Wetherald, 1980: On the distribution of climate change resulting from an increase in CO_2 content of the atmosphere. *J. Atmos. Sci.*, **37**, 99–118, https://doi.org/10.1175/1520-0469(1980)037<0099:OTDOCC>2.0.CO;2.

O'Gorman, P. A., 2010: Understanding the varied response of the extratropical storm tracks to climate change. *Proc. Natl. Acad. Sci. USA*, **107**, 19 176–19 180, https://doi.org/10.1073/pnas.1011547107.

——, and T. Schneider, 2008: Energy in midlatitude transient eddies in idealized simulations of changed climates. *J. Climate*, **21**, 5797–5806, https://doi.org/10.1175/2008JCLI2099.1.

Pavan, V., 1996: Sensitivity of a multi-layer quasi-geostrophic β-channel to the vertical structure of the equilibrium meridional temperature gradient. *Quart. J. Roy. Meteor. Soc.*, **122**, 55–72, https://doi.org/10.1002/qj.49712252904.

Pierrehumbert, R., 1984: Local and global baroclinic instability of zonally varying flow. *J. Atmos. Sci.*, **41**, 2141–2162, https://doi.org/10.1175/1520-0469(1984)041<2141:LAGBIO>2.0.CO;2.

Pithan, F., T. G. Shepherd, G. Zappa, and I. Sandu, 2016: Climate model biases in jet streams, blocking and storm tracks resulting from missing orographic drag. *Geophys. Res. Lett.*, **43**, 7231–7240, https://doi.org/10.1002/2016GL069551.

Polvani, L. M., and P. J. Kushner, 2002: Tropospheric response to stratospheric perturbations in a relatively simple general circulation model. *Geophys. Res. Lett.*, **29**, 1114, https://doi.org/10.1029/2001GL014284.

Ramaswamy, V., and Coauthors, 2001: Stratospheric temperature trends: Observations and model simulations. *Rev. Geophys.*, **39**, 71–122, https://doi.org/10.1029/1999RG000065.

Screen, J. A., C. Deser, I. Simmonds, and R. Tomas, 2014: Atmospheric impacts of Arctic sea-ice loss, 1979–2009: Separating forced change from atmospheric internal variability. *Climate Dyn.*, **43**, 333–344, https://doi.org/10.1007/s00382-013-1830-9.

Stephenson, D. B., and I. M. Held, 1993: GCM response of northern winter stationary waves and storm tracks to increasing amounts of carbon dioxide. *J. Climate*, **6**, 1859–1870, https://doi.org/10.1175/1520-0442(1993)006<1859:GRONWS>2.0.CO;2.

Sun, L., G. Chen, and J. Lu, 2013: Sensitivities and mechanisms of the zonal mean atmospheric circulation response to tropical warming. *J. Atmos. Sci.*, **70**, 2487–2504, https://doi.org/10.1175/JAS-D-12-0298.1.

Tamarin-Brodsky, T., and Y. Kaspi, 2017: Enhanced poleward propagation of storms under climate change. *Nat. Geosci.*, **10**, 908–913, https://doi.org/10.1038/s41561-017-0001-8.

Tandon, N. F., E. P. Gerber, A. H. Sobel, and L. M. Polvani, 2013: Understanding Hadley cell expansion versus contraction: Insights from simplified models and implications for recent observations. *J. Climate*, **26**, 4304–4321, https://doi.org/10.1175/JCLI-D-12-00598.1.

Vallis, G. K., P. Zurita-Gotor, C. Cairns, and J. Kidston, 2015: Response of the large-scale structure of the atmosphere to global warming. *Quart. J. Roy. Meteor. Soc.*, **141**, 1479–1501, https://doi.org/10.1002/QJ.2456.

Voigt, A., and T. A. Shaw, 2016: Impact of regional atmospheric cloud radiative changes on shifts of the extratropical jet stream in response to global warming. *J. Climate*, **29**, 8399–8421, https://doi.org/10.1175/JCLI-D-16-0140.1.

Wills, R. C., and T. Schneider, 2016: How stationary eddies shape changes in the hydrological cycle: Zonally asymmetric experiments in an idealized GCM. *J. Climate*, **29**, 3161–3179, https://doi.org/10.1175/JCLI-D-15-0781.1.

——, and ——, 2018: Mechanisms setting the strength of orographic Rossby waves across a wide range of climates in a moist idealized GCM. *J. Climate*, **31**, 7679–7700, https://doi.org/10.1175/JCLI-D-17-0700.1.

Wu, Y., M. Ting, R. Seager, H. Huang, and M. A. Cane, 2010: Changes in storm tracks and energy transports in a warmer climate simulated by the GFDL CM2.1 model. *Climate Dyn.*, **37**, 53–72, https://doi.org/10.1007/S00382-010-0776-4.

——, R. Seager, M. Ting, N. Naik, and T. A. Shaw, 2012: Atmospheric circulation response to an instantaneous doubling of carbon dioxide. Part I: Model experiments and transient thermal response in the troposphere. *J. Climate*, **25**, 2862–2879, https://doi.org/10.1175/JCLI-D-11-00284.1.

Wu, Z., and T. Reichler, 2018: Towards a more Earth-like circulation in idealized models. *J. Adv. Model. Earth Syst.*, **10**, 1458–1469, https://doi.org/10.1029/2018MS001356.

Yin, J. H., 2005: A consistent poleward shift of the storm tracks in simulations of 21st century climate. *Geophys. Res. Lett.*, **32**, L18701, https://doi.org/10.1029/2005GL023684.

Yuval, J., and Y. Kaspi, 2016: Eddy activity sensitivity to changes in the vertical structure of baroclinicity. *J. Atmos. Sci.*, **73**, 1709–1726, https://doi.org/10.1175/JAS-D-15-0128.1.

——, and ——, 2017: The effect of vertical baroclinicity concentration on atmospheric macroturbulence scaling relations. *J. Atmos. Sci.*, **74**, 1651–1667, https://doi.org/10.1175/JAS-D-16-0277.1.

——, and ——, 2018: Eddy sensitivity to jet characteristics. *J. Atmos. Sci.*, **75**, 1371–1383, https://doi.org/10.1175/JAS-D-17-0139.1.

Zurita-Gotor, P., 2007: The relation between baroclinic adjustment and turbulent diffusion in the two-layer model. *J. Atmos. Sci.*, **64**, 1284–1300, https://doi.org/10.1175/JAS3886.1.

——, and R. S. Lindzen, 2006: A generalized momentum framework for looking at baroclinic circulations. *J. Atmos. Sci.*, **63**, 2036–2055, https://doi.org/10.1175/JAS3737.1.